Application of Fast-Responding Pressure-Sensitive Paint to a Hemispherical Dome in Unsteady Transonic Flow

THESIS

Presented in Partial Fulfillment of the Requirements for the Degree Master of Science in the Graduate School of The Ohio State University

By

Shuo Fang

Graduate Program in Aeronautical and Astronautical Engineering

The Ohio State University

2010

Master's Examination Committee:

James W. Gregory, Advisor

Abstract

The current work focuses on the application of fast-responding polymer/ceramic pressure-sensitive paint (PSP) as an advanced surface pressure measurement technique for the study of unsteady flow fields in large-scale wind tunnels. Three different PSP experimental methods are demonstrated to resolve the surface pressure distribution over a hemispherical dome placed in subsonic flow with freestream Mach number of 0.6 and a total pressure of 71.8 kPa, where the Reynolds Number based on dome diameter (0.254 m) is 2.4 x 10^6. At this flow condition, a predominant shear layer oscillating at 400 Hz over the test model is observed. Three different PSP methods were employed to study this phenomenon: phase-averaged, real-time, and single-shot. In the phase-averaging technique, LED arrays are phase-locked to the shear layer frequency so that the strobed illumination freezes the motion of the oscillating fluid in one instant and the camera shutter stays open long enough to average the fluid motion over many cycles. In the real-time approach, a high-speed camera was used to capture the shear layer frequency at a shutter speed of 10 kHz without any averaging of the images. In the lifetime-based single-shot approach, the PSP information was acquired from one single laser pulse, which was also able to provide instantaneous surface pressures with high spatial resolution. An assessment of the three test methods is presented, with the advantage and disadvantage of each technique evaluated through example.

To study the unsteady fluid dynamic problem in this work using PSP, it is important to demonstrate that the PSP formulation has the capability to accurately resolve the unsteady pressure changes. The response time of the polymer/ceramic PSP was characterized with a dynamic calibration technique using a loudspeaker. The quantitative point-measurement results show that the amplitude response of the PSP behaved like a 4th order dynamic system, with a frequency response of 3700 Hz. The dynamic calibration setup and results are presented.

Dedication

This document is dedicated to my family.

Acknowledgments

It is a pleasure for me to give thanks to all the people and organizations who have helped and inspired me during my graduate studies.

It is difficult to overstate my sincere gratitude to my advisor, Dr. James Gregory, for his enthusiasm, inspiration, and guidance throughout this work. His contributions of time, funding, and ideas helped to make me realize what it takes to be a great researcher, and succeed in life. Furthermore, I would like to thank him for his patience and guidance in my research and during the tough times I had to endure outside of school. I am deeply grateful to be influenced by him.

I am delighted to have interacted with Dr. Mo Samimy by attending his class and having him participate as an active member of my thesis defense committee.

Next, I would like to give a special thanks to Kevin Disotell and Sam Long for all the help they provided me on my experiments at the Air Force Research Laboratory. Among my most memorable experiences over the past few years, the days when we worked together during 3rd shift at AFRL are on the top of the list. Who could forget those stressful nights when we sat in a large empty room from midnight to sunrise, where the only light came from the monitor in front of us, and the only sound we could hear came from the deafening noise of the wind tunnel. Without your help, this thesis would not have been possible.

To all my colleagues in Dr. Gregory's research group, I am sincerely grateful for all the support you have provided me as I set out on my research path. I would like to thank Dr. Thomas Juliano for taking the time to proofread this thesis and providing the critical feedback that helped to refine this document. I would like to thank Di Peng for helping me with the thickness measurements presented in this thesis. I would like to give thanks to all my friends at the lab for providing a stimulating and fun environment in which I could learn and grow.

All of the experiments done on the hemispherical dome were funded by the Air Force Research Laboratory. I would like to thank Robert Guyton for providing us with this great research opportunity. A special thanks goes out to Frank Semmelmayer, who did a top-notch job at overseeing the experiments, making sure everything ran smoothly, and providing me with everything that I needed to make the work presented in this thesis a success. I would also like to thank the wind tunnel workers from Jacobs, who worked tirelessly to operate the wind tunnel and fabricate the parts needed for our experiments.

I would like to thank Tim Bencic at NASA for providing me with the equipments needed for my experiments on the dynamic calibration of PSP.

I would like to thank all of my friends for their encouragement and support. When the times got tough, they were there to listen and talk to. Thanks to everyone who helped to remind me the other aspects of life that are just as important as school.

Lastly, and most importantly, I wish to thank my parents, Li Li and Bida Fang. They raised me, supported me, taught me, and loved me. To them I dedicate this thesis.

Vita

June 2008	B.S. Mechanical Engineering, Wright State University
2008 to 2010	Graduate Research Associate, Department of Aerospace Engineering, The Ohio State University
2010	M.S. Aerospace Engineering, The Ohio State University

Publications

Fang, S.; Disotell, K.J.; Long, S.R.; Gregory, J.W.; Semmelmayer, F.C.; Guyton, R.W., "Unsteady Aerodynamic Application of Fast-Responding Pressure-Sensitive Paint", accepted for publication by *Experiments in Fluids*, in press, DOI: 10.1007/s00348-010-1010-1.

Fang, S.; Long, S.R.; Disotell, K.J.; Gregory, J.W.; Semmelmayer, F.C.; Guyton, R.W., "Comparison of Unsteady Pressure-Sensitive Paint Measurement Techniques", *27th AIAA Aerodynamic Measurement Technology and Ground Testing Conference*, AIAA 2010-4919, Chicago, IL, 2010

Fang, S.; Disotell, K.J.; Long, S.R.; Gregory, J.W.; Semmelmayer, F.C.; Guyton, R.W., "Unsteady Surface Pressure Measurements on a Hemispherical Dome with Pressure-Sensitive Paint", *FLUCOME 2009*, Moscow, Russia, 2009.

Fields of Study

Major Field: Aeronautical and Astronautical Engineering

Table of Contents

List of Figures

Chapter 1 : Introduction to PSP Techniques

In the airplane industry, knowing the aerodynamic forces over the model surface can help scientists predict an airplane's response subjected to equivalent flows. Besides knowing the aerodynamic forces on a particular model, it is also important to understand how those forces are distributed across its entire surface to help further understand specific flow phenomena, and validating computational results. This area is difficult to study because traditional surface pressure measurement techniques can be both expensive and time consuming.

Pressure taps have been used extensively in the past for acquiring surface pressure distributions over test models. The tedious task of drilling large numbers of holes to connect tubing to pressure transducers could take weeks to complete and still may not provide scientists with the spatial resolution they require since these measurements are only made at discrete locations. More advanced techniques than pressure taps involve grid-based computational fluid dynamics (CFD) codes, which provide computer simulations of real world problems. The simulations are performed separating the model surface into grids and calculating the pressure distribution along these grids. Since the resolution of the result depends on the size of grids generated, it may take days to months to obtain a set of good data.

An alternative method for measuring surface pressure is with the use of pressure-sensitive paint (PSP), which is an image-based optical measurement technique with the unique ability to provide surface pressure measurements extended across the entire model at high spatial resolution. Two advantages of using the PSP system are that it is non-intrusive to the flow and can provide higher spatial resolution than conventional techniques, limited only by the pixel resolution of the photodetector. A major objective of the present work is to demonstrate the ability of PSP to resolve high-quality surface pressure data in a large-scale wind tunnel test.

Traditionally, PSP data are acquired using the phase-averaging technique, where the pulsing of LED arrays are phase-locked with the surface pressure oscillations , such as a dominant shear layer, and freezing it at one point in the cycle. The oscillation cycle is averaged over many periods by keeping the camera shutter open long enough to fill the capacity of its sensor. While the averaging scheme helps to increase the signal-to-noise ratio (SNR) in capturing the flow variations at a certain dominant frequency, it also averages out any pressure gradients oscillating at other frequencies. Furthermore, the length of time required to obtain one set of data using this method could introduce significant errors caused by model movement, temperature variations, and intensity deterioration of the luminophore due to an extended period of exposure to the illumination source, also known as photodegradation.[1] For studies that involve complex surface pressure variations, using only the phase-averaging technique may not be enough.

The real-time method involves the use of a high-speed camera with a frame rate high enough to capture all the flow oscillations in real time, without the use of any averaging scheme. This method can capture details in the flow that are missed by the phase-averaging technique, while lowering the errors caused by photodegradation due to its quick data acquisition time. The main downside is the low SNR due to the fast shutter speed. In order to address this issue, a large number of illumination sources must be used.

In the single-shot lifetime method, all the luminescence is collected within one laser pulse, where any effect of model movement is dictated by the lifetime of the luminescence decay. Ideally, all the necessary pressure information can be obtained within a single lifetime decay curve of the PSP formulation. Often, some faster sensor (such as a pressure transducer or position encoder) is needed in conjunction with the PSP to determine the oscillation phase for each image. Although PSP data acquired using the lifetime technique has the ability to capture both the pressure and reference images on the same decay curve from a single laser pulse, a wind-off image is still needed due to point-to-point variations in the paint calibration.

Each of these PSP data acquisition techniques have their own advantages and disadvantages that can provide scientists with different information about the surface pressure distribution. This thesis focuses on the application and comparison of the three different PSP data acquisition methods to the study of unsteady pressure fluctuations on a hemispherical dome placed in subsonic flow.

Chapter 2 : PSP Mechanisms and Methodology

This chapter provides an overview of the working mechanisms of pressure-sensitive paint and their applications to aerodynamic testing. More detailed descriptions of the phase-averaging, real-time, and single-shot lifetime methods are discussed.

2.1 Pressure-Sensitive Paint

Overview

PSP is an image-based optical measurement technique used for measuring the global surface pressure distribution over aerodynamic models. The PSP technique is based on luminescence of oxygen-sensing molecules, known as luminophores, which are dispersed throughout a permeable paint binder. Extensive reviews of PSP can be found in the general literature[2-5], and an overview will be provided here. When the luminescent molecule absorbs a photon from a short-wavelength light, it is excited to a higher-energy state. The molecule recovers to its initial state by emitting longer-wavelength light through radiative decay. This property of luminescence is known as Stokes shift. Variation in the intensity of the emitted light results when an excited luminophore molecule transfers some of its higher energy level to the surrounding oxygen molecules; this process is known as oxygen quenching. Since oxygen quenching is dependent on the concentration of oxygen molecules, as the partial pressure of oxygen increases, the luminescent intensity will decrease. Figure 2.1 shows the absorption and emission spectrum for platinum meso-tetra (pentafluorophenyl) porphine (PtTFPP).[6]

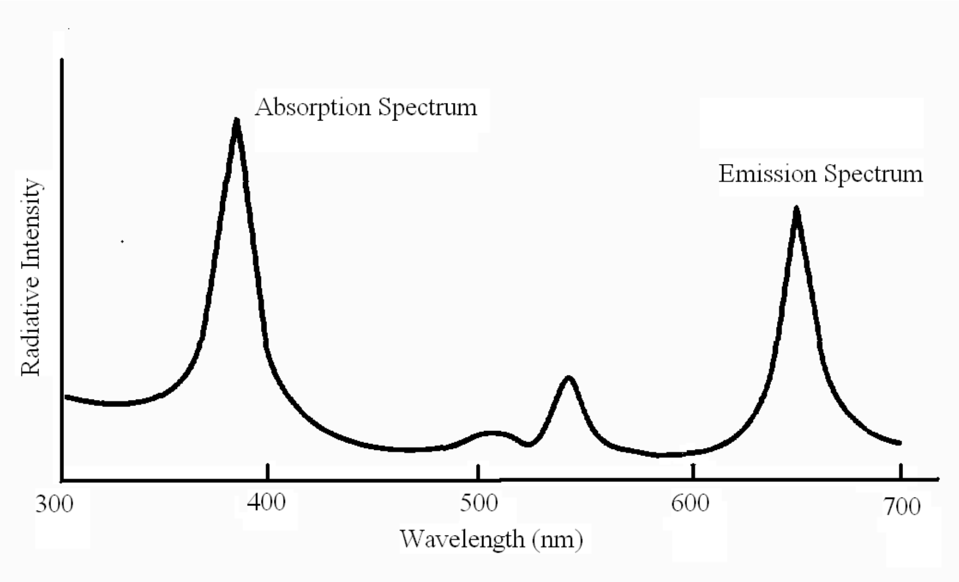

Figure 2.1. Absorption and Emission Spectra for PtTFPP[6]

A typical PSP setup is shown in Figure 2.2, which includes the test model with PSP applied over it, an excitation source, and a photodetector with an optical long-pass filter placed in front of the lens[7]. The PSP distributed over the aerodynamic model is excited by a light source such as a LED array or laser, and the luminescent intensity is collected using a photodetector such as a CCD camera or photomultiplier tube (PMT). In the case of a camera, each pixel acts as a pressure tap, allowing for high resolution data of the surface pressure distribution.

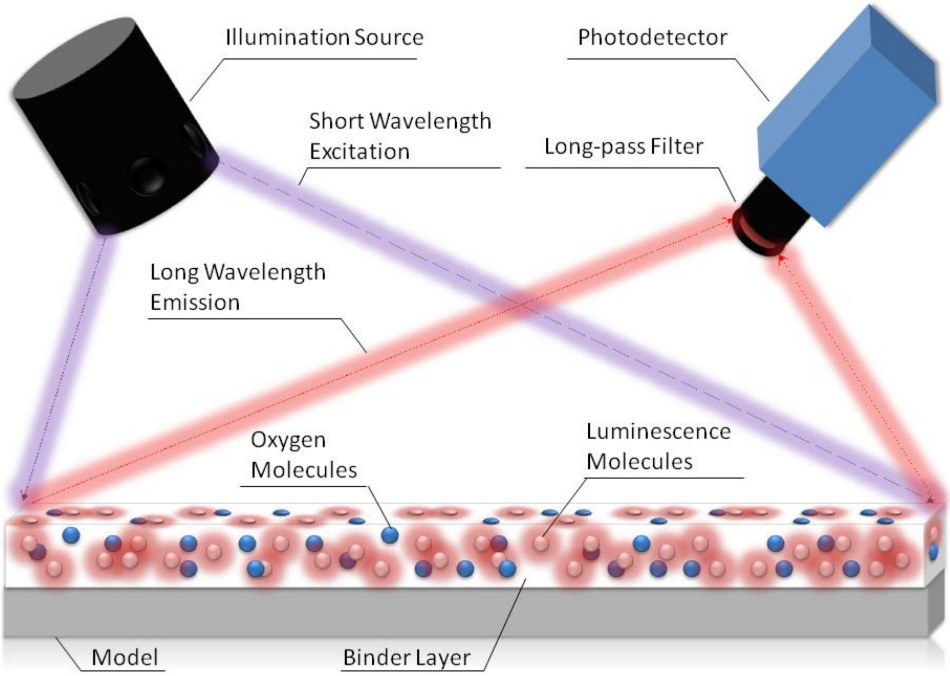

Figure 2.2. Basic PSP Setup

The recorded light intensity data can be converted to pressure data using several methods. For this study, both intensity-based and time-based methods were employed, where the pressure is derived by taking the ratio of the luminescent intensity of the paint at the test (*wind-on*) condition over the luminescent intensity of the paint at the reference (*wind-off*) condition. The luminescent intensity of the PSP is inversely related to the concentration of oxygen, and is described by the Stern-Volmer relation in Equation (2.1):

$$\frac{I_{ref}}{I} = A(T) + B(T)\frac{P}{P_{ref}} \tag{2.1}$$

where P and I are the pressure and luminescent intensity at the wind-on condition, P_{ref} and I_{ref} are the pressure and luminescent intensity at the wind-off condition. The values $A(T)$ and $B(T)$ are temperature-dependent calibration coefficients that are experimentally determined. By taking the ratio of the luminescent intensities at wind-on and wind-off conditions, errors caused by non-uniform illumination and variations in the PSP coating may be eliminated. According to the Stern-Volmer equation, the PSP will have the highest luminescence when there is the least amount of oxygen concentration.

Calibration

In order to obtain the surface pressure of the aerodynamic model using PSP, a relationship between the luminescence intensity of the PSP and air pressure must be experimentally determined through either *a priori* or *in situ* calibration process. Typically, an *a priori* calibration involves placing a PSP sample inside of a pressure chamber where the pressure can be adjusted while holding the temperature constant.[8] The emission signal is then collected by a photodetector over a range of pressures to obtain a relationship between the intensity ratio and the pressure ratio. Finally, this calibration is applied to the intensity ratio at the test conditions to obtain the surface pressure distribution. In the case of *in situ* calibrations, an array of pressure taps is placed across the test model surface and the PSP intensity values are obtained in the immediate vicinity of these taps.[8] Values of the PSP intensity ratio I/I_{ref} are calibrated against the pressure ratio P_{ref}/P obtained from the pressure taps during the test conditions. The calibration constants for the Stern-Volmer equation are determined from the linear fits of this data.

Photodegradation

One drawback of using PSP is the phenomenon of photodegradation, where the luminescent intensity of the PSP deteriorates over time as the molecules are over-exposed to high intensities of light for an extended period of time. During the post-processing stage the change in intensity signal between each individual image may cause significant errors if one image is acquired long after the previous. Therefore, efforts must be taken to minimize photodegradation when designing an experiment involving PSP. In general, each set of data should be obtained using the least number of light flashes required to fill the camera sensor cavity so that the paint is not over-exposed to the excitation light.

2.2 Measurement Techniques

Uncertainties

As discussed earlier, PSP is an image-based measurement technology where the basic system involves excitation sources and photodetectors. The surface pressure measurement is obtained after applying the calibration, obtained experimentally, to the PSP luminescent signal over the model surface after the excitation light has been filtered out. Some typical excitation sources include LED arrays, high-power lasers, and xenon lamps. Typical photodetectors include scientific-grade cameras (CCD or CMOS), photo-multiplier tubes (PMT), and photo-diodes.

For the intensity-based PSP measurements discussed in this work, it is important that the luminescent intensity remains uniform over the entire surface of the model to minimize any errors caused by these spatial variations. Theoretically, this error can be minimized by taking the ratio of wind-off and wind-on intensities since this ratio is a function of the local pressure only. In application, however, the luminescent output also depends on variations in the excitation source and temperature variations[5]. Unfortunately, PSP's sensitivity to temperature variations is one of its major sources of errors, where the intensity of the luminescent output varies with temperature changes. Some other sources of errors in PSP measurements include model displacement and deformation, dust and oil blown over the model during testing, and noise sources from the cameras.

Since an intensity-based method is employed, where the pressure is derived from a ratio of wind-on and wind-off images, model movement between the two conditions must be minimized in order to extract accurate pressure data, otherwise significant error can be introduced as false pressure changes. When model movements do occur, image registration techniques are required to minimize such errors by matching the two images to the closest pixel. It has been stipulated that the registration error should be less than half a pixel.[9]

Phase-averaging Method

The phase-averaging method has been proven to be an effective method to increase the SNR for unsteady flow measurements.[10] The SNR of the PSP data is increased by averaging a number of images taken at the same instance in the periodic pressure variations, excited by LED arrays phase-locked to the flow feature oscillating at the dominant frequency. This method can be easily applied to a steady flow field, but since the unsteady flow field has a broad frequency range and random amplitude fluctuations, the signal must be heavily filtered to lock on to the flow characteristics at the frequency of interest. Two of the main causes of error with this method come from the illumination variation between image to image and due to model movement between wind-on and wind-off images.

Real-time Method

The real-time data acquisition method involves use of a high-speed camera with shutter speeds capable of capturing high-speed flow changes. Although this method eliminates the need for sophisticated triggering instrumentation, it does require a large amount of continuous excitation light to fill the camera sensor due to the fast shutter speed. The advantage of this method is that detailed real-time information of the flowfield can be acquired within a very short amount of time, minimizing effects of temperature variations and photodegradation, but the tradeoff is the very low SNR and spatial resolution due to the fast shutter speed.

Lifetime Method

The lifetime method is based on the response of the luminescent lifetime to an excitation source.[8] A schematic of this technique is shown in Figure 2.3. For the single-shot variation of this method, the paint is excited to a higher energy level by a single illumination pulse and all of the luminescence is collected by a photodetector within that brief moment. Typical excitation sources include LED arrays or a high-power laser. Two images are acquired during this short pulse of light, where one image is taken during the illumination pulse and the second is collected during the decay of the luminescence. In Figure 2.3 (Dr. Jim Crafton, ISSI), *gate 1* (G1) serves as the reference state since it is relatively insensitive to pressure and *gate 2* (G2) is sensitive to pressure since it is acquired when the paint is in the process of returning to the ground state. The timing of these gates is optimized such that pressure sensitivity is maximized while maintaining a favorable SNR. By applying a calibration to the ratio of the two gates, the surface pressure distribution can be obtained.

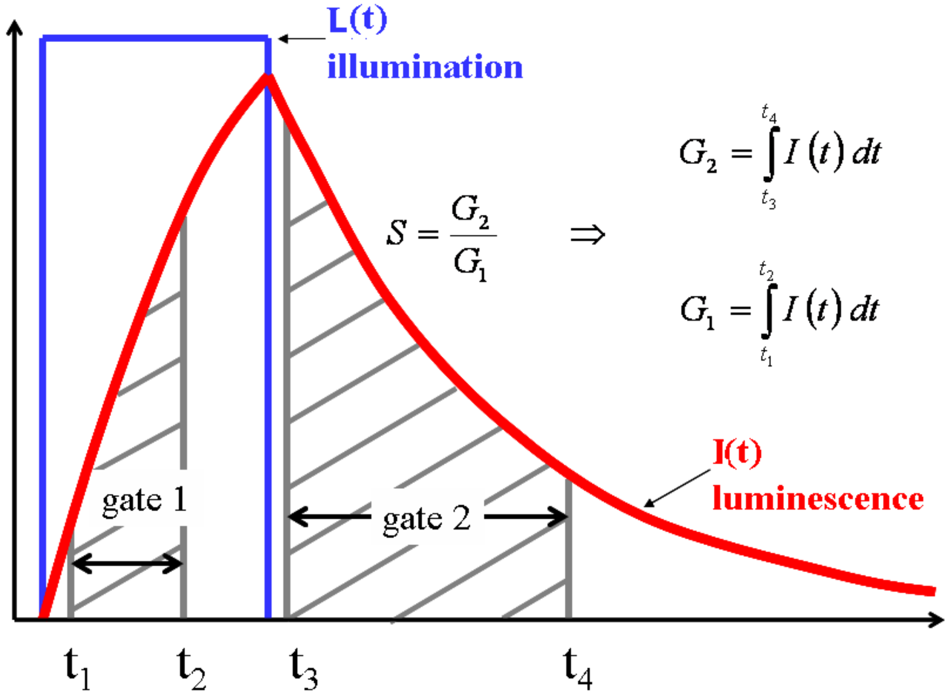

Figure 2.3. Representation of Lifetime-based PSP Technique (Dr. Jim Crafton, ISSI)

The major advantage to the single-shot lifetime method is the minimization of photodegradation since all of the required data can be obtained within one short burst of excitation light. Theoretically, all of the pressure information can be obtained from the ratio of the two gates within one decay curve since the lifetime of the paint at a uniform pressure and temperature should remain constant at each point on the model. However, it has been shown that a major source of error in the lifetime-based pressure measurements is due to pixel-to-pixel variations of the paint calibration and temperature variations over the surface of the model.[7, 11] Although the source of the noise in the image obtained at G1 is unclear, it has been shown that by taking a wind-off ratio can help to eliminate this noise.

2.3 Previous Work

As stated earlier, the phase-averaging method has been used extensively in the past for both steady and unsteady PSP measurements. Gregory et al. reported on the dynamic calibration results for several different PSP formulations using a fluidic oscillator.[12] The results showed that the frequency response of polymer/ceramic PSP (PC-PSP) was at least 20 kHz. Gregory also reported on the application of polymer ceramic PSP for measuring the unsteady surface pressures on a turbocharger compressor blade.[13]

Acquiring PSP data using the real-time method with high-speed cameras and continuous illumination has many limitations due to its poor SNR. Nakakita used a high-speed camera to record the pressure fluctuations on a circular cylinder.[14] Many experiments have been documented using high-speed cameras in shock tubes and hypersonic tunnels with large pressure gradients.[15, 16]

The conventional lifetime method was qualitatively demonstrated in 2005 for 15% scale swept tip rotor blades, where the 15% of each blade was painted with PSP.[17] Recently in 2010, Wong et al. made further developments on this technique by validating the PSP measurements with pressure taps for the rotor blade surfaces.[18] Gregory et al. used the lifetime-based single-shot PSP technique to study a rotor blade and an airfoil in an oscillating freestream.[19] Kumar also demonstrated the surface pressure measurements on rotating surfaces with unsteady pressure fluctuations using the lifetime-based single-shot methods.[20]

Chapter 3 : PSP Characterization for Large-Scale Wind Tunnel Test

In order for PSP to be a valid surface pressure measurement technique, the paint must be sensitive enough to capture the pressure gradients over the model surface. Furthermore, the PSP formulation is required to have a frequency response high enough to resolve the unsteady pressure fluctuations on the surface of the test model. With the objective to obtain time-resolved high-resolution pressure data over a hemispherical dome placed in subsonic flow, some of the known and widely used fast-response paints have been investigated. In the following sections, detailed discussion of requirements and improvements of paint performance is provided. The objective of this investigation is to identify a suitable paint formulation for all three of the data acquisition techniques in unsteady test conditions.

3.1 Frequency Response of Pressure-Sensitive Paints

The response time of PSP has been found to be dependent on the lifetime of the luminescent decay and the time scale of oxygen diffusion within the paint binder.[21,22] In the past, much effort has been put into investigating the lifetime of different luminophore formulations and increasing the oxygen permeability of the binder layer.

Luminophore Lifetime

As mentioned previously, the basic mechanism behind PSP can be summarized as a process where the sensor molecules are excited to an elevated energy state, when illuminated with a light source at an appropriate wavelength. The process of luminescence can be described by the Jablonski Energy Level Diagram in Figure 3.1[23], which shows the energy level (represented by the height), above the ground state S_0, of each excited state of a luminophore molecule. The electrons of each molecule are arranged in a different combination of the electron orbits and spin orientations in each state, where the states are divided into a singlet system (e.g. S_0, S_1, S_2) and a triplet system (T_1, T_2) which represent the different spin orientations.[3]

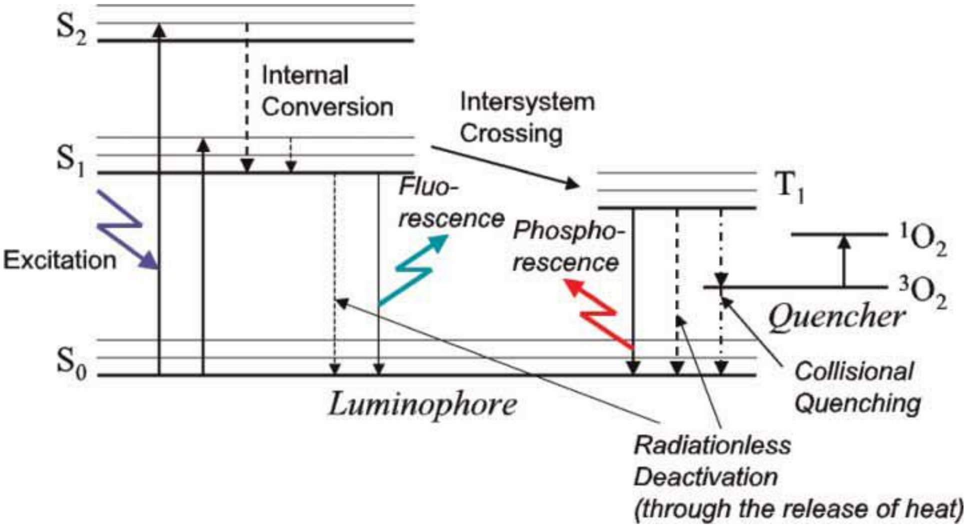

Figure 3.1. Jablonski Energy Level Diagram[23]

The excited luminophores return to the ground state through a combination of radiative (luminescence) and radiationless decay processes. Luminescence, or fluorescence is when the photon emission occurs between states of the same spin state (e.g. from S_1 to S_0). Radiationless emission (energy loss), or phosphorescence, occurs if the spin state of the initial and final energy levels are different (e.g. from T_1 to S_0). Radiationless processes include oxygen quenching and energy transfer. The major photophysical mechanism for PSP is oxygen quenching, where the excited energy of the sensor molecules is transferred to the surrounding oxygen molecules. As a result, the luminescent intensity is reduced with increasing oxygen concentration.

The lifetime of a PSP formulation is the mean time required for the luminescent molecules to return to their ground state after being excited to a higher energy level, and can be described by the given reciprocal of the rate constant of the corresponding process. The response of the luminescent emission, after being excited by an excitation source, can be described as a first order system,

$$I(t) = Ae^{-\frac{t}{\tau}} \tag{3.1}$$

where τ is the luminescent lifetime of the paint, I is the luminescent intensity, t is the elapsed time, and A is a constant. The lifetime constant, τ, can be calculated by statistically fitting the luminescent intensity values as an exponential curve. An alternate way of obtaining the lifetime constant is to take the inverse of the slope of the linear relationship between the natural log of I and t. From (3.1), we get

$$\ln(I) = -\frac{1}{\tau}t + \ln(A) \tag{3.2}$$

The lifetime of luminescent molecules is an important property to consider before conducting an experiment using PSP methods because camera exposures are dependent on this parameter. If the lifetime of the paint is of the same order as the oscillation period of the pressure gradient over the test model, significant blurring will be observed in the PSP data. This blurring is due to insufficient frequency response to the unsteady pressure changes since a luminescent molecule will not react to pressure changes until the molecule has relaxed back to its ground state. Therefore, the lifetime of the luminophore should be at least two orders of magnitude faster than the pressure oscillation frequency of interest.

Pressure Sensitivity

Pressure sensitivity (*SP*) is a measure of the minimum change in pressure that can be resolved by PSP and is defined as[5]:

$$SP = \frac{\Delta\left(I_{ref} / I \right)}{\Delta P} \tag{3.3}$$

A higher value of SP indicates a larger luminescent intensity variation resulting from the pressure gradient. This characteristic is important when selecting different paint formulations for PSP experiments involving small pressure changes.

Common Luminophores

The three main types of luminophores commonly used in PSP applications are shown in Figure 3.2; they include metalloporphyrin, ruthenium complexes, and pyrene derivatives.[3] A short description and their characteristics are provided below.

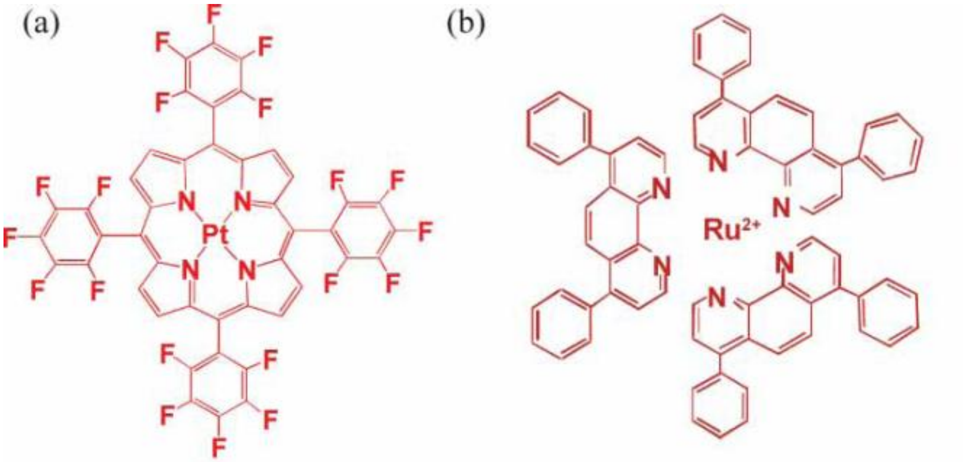

metalloporphyrin
(PtTFPP)

transition metal-ligand comprex
($[Ru(dpp)_3]^{2+}$)

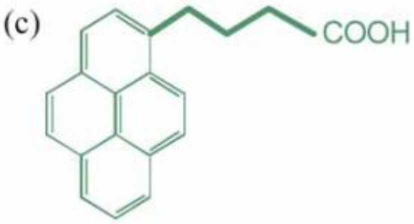

polycyclic aromatic hydrocarbon
(pyrene-1-butylic acid)

Figure 3.2. Common Luminophores[3]

Metallophorphyrins arecompounds formed by a combination of a porphyrin with a metal. Platinum tetra (pentafluorophenyl) porphine (PtTFPP) is a type of metallophorphyrin widely used in current PSP measurements. It has a high-quantum yield of phosphorescence emission and is very sensitive to oxygen.[3] It has a maximum absorption spectrum at 392 nm and a maximum emission wavelength is 650 nm. The lifetime of PtTFPP at atmospheric conditions is about 10 μs, which is much longer than the lifetimes of ruthenium complexes and pyrene derivatives. [24]

Ruthenium is a rare transition metal of the platinum group, with some of its complexes used as optical sensors for oxygen. $[Ru(dpp)_3]^{2+}$ is a ruthenium (II) complex commonly used for PSP measurements. $[Ru(dpp)_3]^{2+}$ exhibits many advantageous traits that make it a great luminophore for PSP measurements, including a single emission peak, high oxygen sensitivity, and photochemical stability. With an absorption spectrum peak at 500 nm and a broad absorption band, a variety of blue or green illumination sources can be used for excitation of the luminescent molecules. $[Ru(dpp)_3]^{2+}$ has been shown to have a lifetime of around 0.13 μs at atmospheric conditions.[25] However, a drawback of using this luminophore is its large temperature sensitivity.

Pyrene derivatives are often used in PSP measurements. Oxygen quenching plays a vital role in relaxing the luminescent molecules to ground state due to its longer fluorescence lifetime (~200 ns). Pyrene derivatives have been found to have strong fluorescence traits with high quantum yield and low temperature sensitivity.[26] However, they usually suffer from severe degradation due to sublimation/evaporation or UV irradiation.[27]

PSP Binder

The binder layer of the PSP provides a surface in which the luminescent molecules can be attached to the surface of the test model. As stated earlier, the frequency response of PSP can be limited by either the lifetime of the luminescent decay, or by the time scale of oxygen diffusion within the binder layer. In most cases luminophore molecules with sufficiently short lifetimes can be selected, such that the frequency response is limited by only the binder characteristics. Conventional PSP binder formulations are polymer-based, which results in a slow response time for pressure changes on the order of seconds. The frequency response characteristics of polymer-based PSP therefore limit its application to mainly steady measurements.

The response time of PSP is directly related to the rate of oxygen diffusion (τ_{diff}) within the paint layer, which is governed by two key parameters. The first is the paint layer thickness (h) and the second is the diffusion coefficient (D_m), which is a measure of the binder porosity. The paint response time is related to these properties by

$$\tau_{diff} \propto \frac{h^2}{D_m} \tag{3.4}$$

Based on the relationship in (3.4), the time response of the PSP can be improved by either decreasing the binder layer thickness or by increasing the diffusivity of the binder. Both cases have been studied extensively in an effort to produce a fast-responding PSP formulation that outperforms conventional polymer-based paints.[28-31] Although decreasing the paint layer thickness may yield a greater improvement on the response time, it would also imply lesser luminescence emission which would result in a decrease in SNR. Therefore, an optimal thickness exists for all PSP paint formulations. To further increase the time-scale of diffusivity and increase PSP frequency response, a fast-responding formulation known as porous PSP has been developed with the objective of increasing oxygen diffusivity within the binder layer. A schematic comparison between the oxygen quenching process of conventional polymer-based PSP and porous PSP is shown in Figure 3.3 below.[32] In the figure, the paired dots represent oxygen molecules and the single dots represent luminophore molecules.

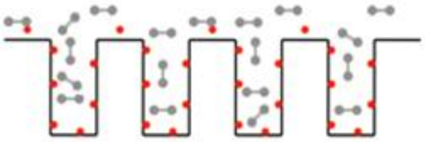

Fast PSP has open pores that increase surface area. Active probe sits on the surface and Oxygen has direct access to the probe.

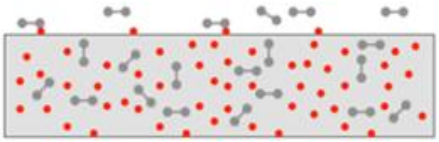

Regular PSP requires that the Oxygen diffuse through the binder to the active probe. The diffusion process is much slower.

Figure 3.3. Comparison of Porous and Conventional PSP[32]

For oxygen quenching to take place in conventional polymer-based PSP, oxygen molecules must permeate into the binder in order to interact with the luminescent molecules, causing a delay in the response to pressure changes. In contrast, the porous binder allows the luminescent molecules to be more “open” to the test gas so that they can interact freely with the oxygen molecules, decreasing the response time dramatically. At the same time, the porous binder provides a large effective surface area, improving luminescent intensity and increasing the SNR of the PSP images. Extensive information on the chemistry, applications, and data reduction techniques of polyer-based and porous PSP has been reviewed in the literature.[3, 5] There are many different types of porous PSPs in use, with different types of binders. Some common porous binders include thin-layer chromatography plate (TLC-PSP), anodized-aluminum (AA-PSP), and polymer-ceramic (PC-PSP).

The TLC plate consists of a thin layer of absorbent material, usually silica gel, aluminum oxide, or cellulose applied over a sheet of glass, plastic, or aluminum foil. The luminophore is applied to the plate by either dipping or spraying and stays on the plate via intermolecular force. TLC-PSP has been shown to achieve submillisecond response times by using a commercial porous silica-gel TLC plate.[33] However, TLC-PSP is fragile and limited to use on flat plates.

The AA-PSP was developed by Asai et al.[29] and was later improved by Sakaue[34]. Anodized aluminum is formed through an electro-chemical process that causes the surface of the aluminum to oxidize. This oxidized aluminum, in which there are large numbers of micropores, forms a strong coating as it replaces the original aluminum on the surface. Like the TLC-PSP technique, luminophore can be applied to the anodized aluminum layer using dipping or spraying methods. Although AA-PSP can be applied to curved surfaces and is not as fragile as TLC-PSP, the procedure of forming the anodized aluminum layer can be difficult.[34]

The polymer/ceramic PSP is a composite formulation aimed specifically at improving the diffusivity of the binder layer. A high concentration of ceramic particles is mixed with a small amount of polymer to help hold the ceramic particles to the surface of the test model. The porous surface formed by the ceramic particles act as the binding locations for the luminescent molecules. In earlier works, the polymer/ceramic mixture was applied to a Mylar film through a tape casting process.[35] Later, Gregory developed a sprayable formulation by diluting the solution with distilled water, but still maintaining the low polymer weight fraction.[13] The polymer/ceramic layer can be applied on the model surface using airbrushing techniques. The luminophore solution, dissolved in methanol, is then oversprayed on the polymer/ceramic binder. Gregory's sprayable form of PC-PSP has been shown to exhibit response times as low as 25μs.

3.2 PSP Considerations for Wind-Tunnel Test

A combination of the sprayable PC-PSP binder layer and PtTFPP luminophore are considered for the application in this work to resolve the unsteady high frequency contents over a hemispherical dome placed in Mach 0.6 flow. The main reasons for choosing this combination are the fast response of the binder layer and the high pressure-sensitivity of the luminophore. High pressure-sensitivity is necessary because there are areas on the model with small pressure gradients. General paint preparation recipes can be found in literature[5]. The paint recipes relevant to this work are provided below. Paint application techniques are also discussed.

Paint Application

Two main pressure-sensitive paint application techniques include spray coating and dip coating. Spray coating involves the use of an airbrush that atomizes the paint mixture to apply the paint uniformly across the model surface. Spray coating can also be used for the application of luminophore solutions. Dip coating involves submerging a test model, already covered in binder layer, into a luminophore solution to evenly distribute the luminophore on the model. Due to the large size of the test model studied in this work, an airbrush was used to apply the paint evenly over the model.

PSP Preparation

Two steps are required in preparing the PC-PSP. First, a ceramic slurry solution is prepared by mixing distilled water with 12 milligrams of ceramic dispersant (Rohm & Haas D-3005) and 1.7 grams of Titanium-dioxide (TiO_2) particles per gram of water. After ball-milling the slurry solution for an hour, Rhoplex HA-8 (Rohm & Haas) is then added by a weight fraction of 3-4%. After several minutes of stirring, three to four coats of this paint binder are airbrushed over the model surface and allowed to dry for several minutes. The second step involves preparation of the PtTFPP luminophore solution. The Pt(III) meso-tetra(Pentaflourophenyl) porphine powder (Frontier Scientific, Inc.) is dissolved in dichloromethane to form the luminophore solution. Using similar airbrushing techniques, three to four coats of this luminophore are sprayed over the binder layer on the model surface.

3.3 PSP Calibration

As discussed earlier, calibration of PSP luminescence data to pressure data can be performed either *a priori* or *in situ*. These static calibrations determine the sensitivity of the paint response by relating the luminescence ratio to the pressure ratio or relating the pressure to the lifetime decay (τ). Another set of calibration techniques called dynamic calibrations are aimed at determining the paint frequency response by comparing the amplitude attenuation and phase shifts at different frequencies. Discussions on both calibration techniques are provided below, along with dynamic calibration data for PC-PSP oversprayed with PtTFPP luminophore.

Static Calibrations

Typical *a priori* Stern-Volmer static calibrations are performed using small metal sheets, or coupons, applied with the same PSP formulation used on the test model. This coupon is placed in a pressure chamber specifically designed for this purpose. The paint is excited with an illumination source and the luminescent intensity is captured with either PMT or a CCD camera at a series of pressures relevant to the test conditions.

The luminescent intensity ratio versus the normalized lifetime decay for $[Ru(dpp)_3]^{2+}$ polymer/ceramic (Ru-PC) PSP and PtTFPP polymer/ceramic (Pt-PC) PSP are shown in Figure 3.4 and Figure 3.5, respectively.[20] The constant τ_{ref} represents the lifetime of the paint formulation at atmospheric conditions. The images show that the luminescence lifetime (τ) decreases with increasing pressure. Comparing the images for both paint formulations, it can be seen that although Ru-PC has a shorter lifetime decay than Pt-PC, it is far less sensitive to pressure changes. Kumar reported that the pressure sensitivity of Ru (bpp) in polymer/ceramic is 0.11% per kPa, and that of PtTFPP in polymer/ceramic is 0.52% per kPa.[20] From these findings, the conclusion can be made that PtTFPP is more favorable than Ru (bpp) in polymer/ceramic in applications where pressure variations are small, such as small pressure gradients caused by the shear layer vortices on the hemispherical dome described in this work.

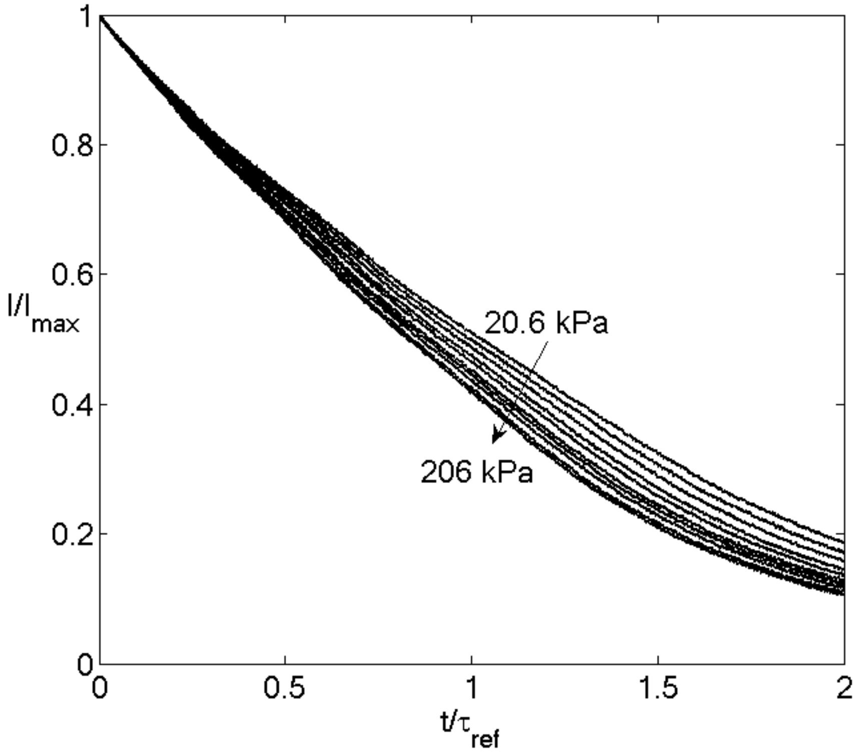

Figure 3.4. Luminescence Decay Curves for Ru-PC Paint[20]

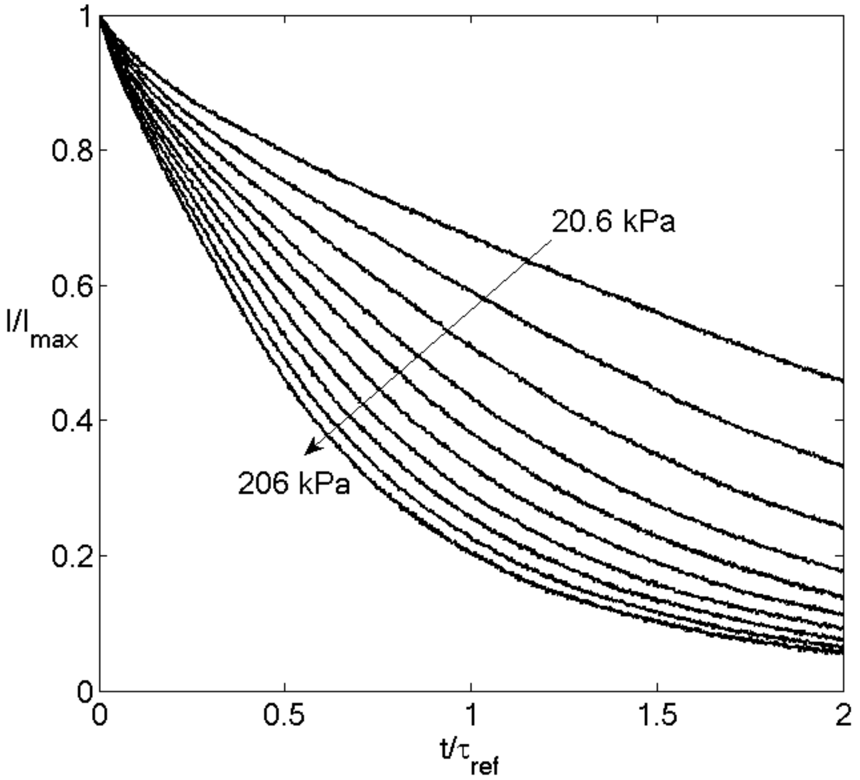

Figure 3.5. Luminescence Decay Curves for PtTFPP-PC Paint[20]

Dynamic Calibrations

Many engineering tests involve the study of unsteady flow phenomena around bluff bodies such as shear layers and shedding of vortices. It is therefore important to have instrumentation that can respond quickly enough to accurately resolve unsteady pressure changes. In recent years, with the development and application of porous PSP to the study of unsteady fluid dynamic problems, there is an increasing need for accurate characterization of the response time of PSP. Ideally, dynamic calibrations should be able to provide information about the signal amplitude and phase difference as a function of frequency. Many dynamic calibration methods been developed to meet this need, including shock tube facilities[37], solenoid valves[38], loudspeakers[39], periodic shock wave generators[39], siren pressure generators[40], and fluidic oscillators.[12] Due to the large frequency range of the loudspeaker, it was selected for the frequency response calibration of the PtTFPP polymer/ceramic PSP in this work. As mentioned earlier, the frequency response depends on the paint layer thickness. For reference purposes, a profilometer (Dektak II A) was used to measure the thickness of the paint formulation, which was found to be 28.4 μm. The plot obtained from the profilometer is shown in Figure B.1 in Appendix B.

3.4 Dynamic Calibration Using Loudspeaker

Dynamic characterization of a pressure sensor can be executed experimentally by subjecting it to a periodic pressure. The frequency response of a pressure-sensitive paint can be obtained by using a periodic pressure generator with varying frequency. A loudspeaker is an excellent device for the dynamic calibration of pressure-sensitive paint because of its large frequency range. It consists of a sound source that generates an oscillating sound pressure wave in a small test chamber. As these pressure waves propagate down the test cell, a pattern of standing waves is created. Knowing the signal from a reference pressure transducer, researchers can obtain the phase delay and amplitude attenuation in the frequency domain. The advantage of using the loudspeaker is that it can be driven up to large frequencies, on the order of tens of kilohertz. The disadvantage of such a setup is the low amplitude of the pressure fluctuations, which is on the order of 150 dB.[3]

Experimental Setup

For dynamic calibration of the pressure-sensitive paint, a loudspeaker is used to provide acoustic pressure oscillations in a closed pipe. A transparent pipe is used in this experiment to allow the excitation source to reach the PSP sample inside the pipe and allow the PMT to collect the PSP response. The setup for this experiment is shown in Figure 3.6. The setup consists of a loudspeaker (Community M4 Professional Loudspeaker) placed at one end of an enclosed pipe at atmospheric conditions. A cap with a pressure transducer mounted in the middle and painted with PtTFPP PSP closes the other end of the tube. The cap is tightly fitted in the tube to prevent it from mechanically vibrating from the sound wave.

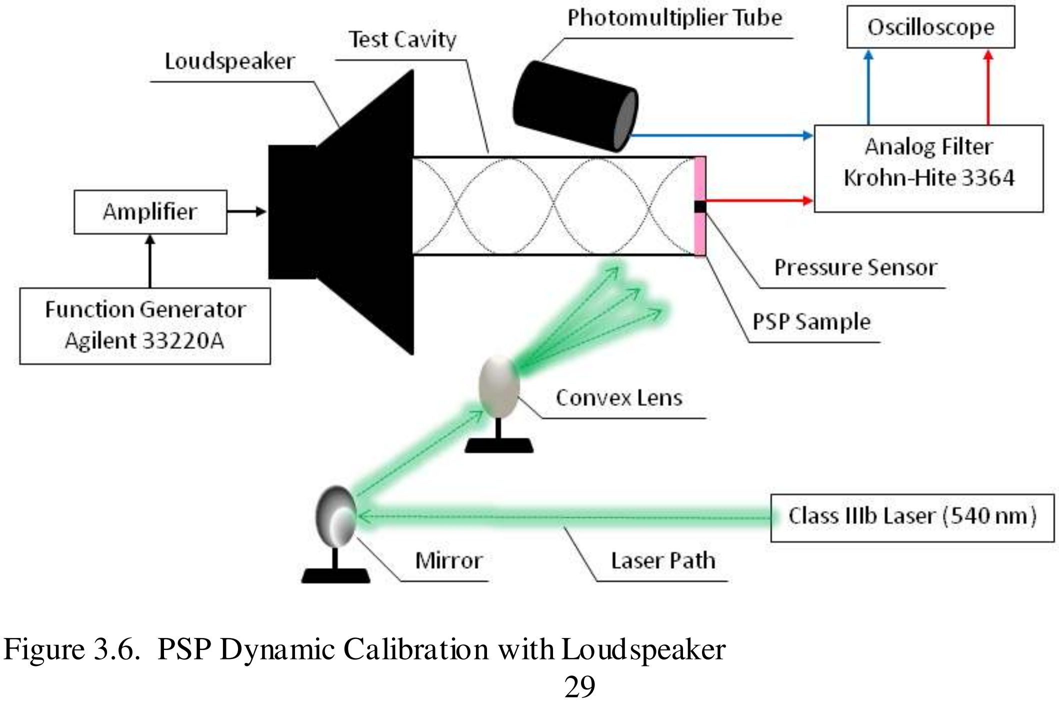

Figure 3.6. PSP Dynamic Calibration with Loudspeaker

The loudspeaker is driven by an amplifier (Carver PXm450) and a function generator (Agilent 33220A). The function generator allows the experimenter to provide a series sine waves with known frequencies and amplitudes to drive the speaker. The acoustic waves from the loudspeaker produce pressure waves within the tube, which are measured using a pressure transducer mounted flush to the painted side of the end cap. The signal of the pressure transducer is used as a reference. Since the pressure waves are small, a piezoresistive pressure transducer (Endevco 8507C-1) with a 1-psi full-scale range was used.

As shown in Figure 3.6, continuous illumination from a class IIIB laser (Crystalaser CL-2000) with a spectral output peak of 540 nm is used to excite the PSP. The excitation laser is reflected by a mirror and diffused through a convex lens (both provided by Thorlabs) to create a laser illumination volume that spread uniformly over the PSP-coated side of the end cap. As the PSP responded to the oscillating sound wave, its phosphorescence modulated at the frequency of the sound. A Thorlabs convex lens is used to collect and focus the phosphorescence onto a Hamamatsu photomultiplier tube (PMT). The emitted light detected by the PMT is isolated by a 650 nm bandpass interference filter that rejected stray and scattered light.

An analog filter with a lowpass cutoff frequency of 200 kHz provided a voltage gain of 40 dB to both the PMT and the pressure transducer signals. The readout voltages were collected by a digital oscilloscope (Lecroy Waverunner 44Xi). The frequency of the input waveform was swept from 420 Hz to 5000 Hz. Since the detected pressure changes in the tube are small, only data at resonant frequencies is recorded. The resonant frequencies are those that have maximum amplitude within a certain frequency range. By comparing the root-mean square values of both signals, the frequency response of the PSP can be determined.

Data Reduction and Results of Dynamic Calibrations

The readout voltages from the PMT and the pressure transducer are averaged over 200 sweeps by the oscilloscope and collected at resonant frequencies between 420 Hz and 5000 Hz. Figure 3.7 shows the response of the pressure transducer and the PSP, both converted to units of psi, to a 420 Hz sound wave. Similar plots at other resonant frequencies can be found in Appendix A. As expected, the PSP signal is much noisier than the signal from the pressure transducer. Since the noise of the PMT can be described in terms of the photon shot noise, the SNR is roughly proportional to the square root of the number of photoelectrons collected.[41]

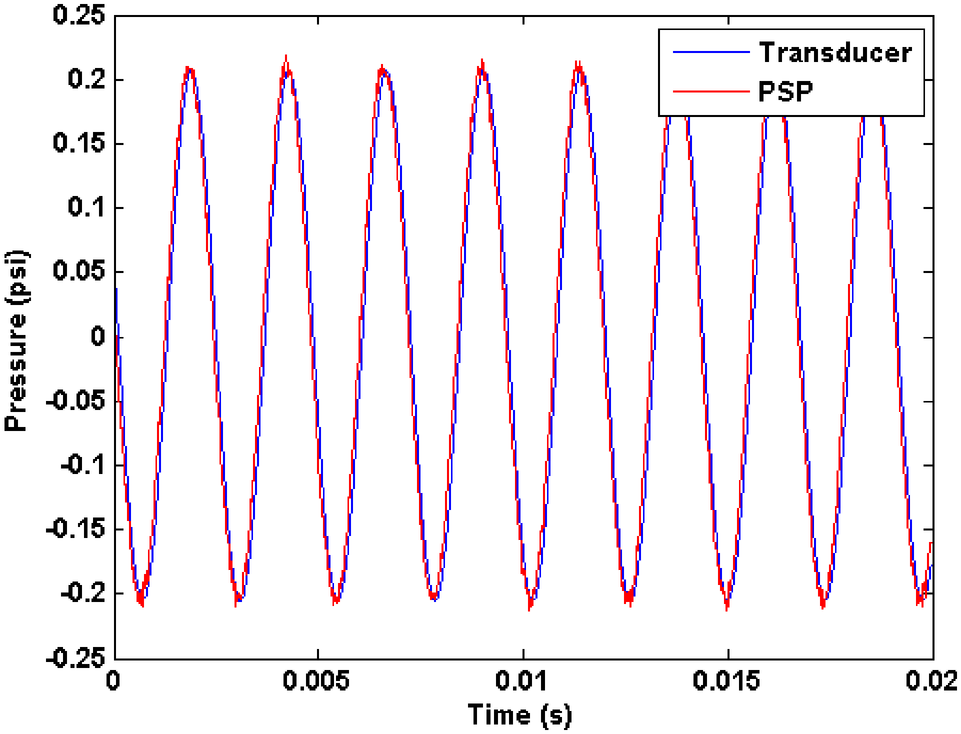

Figure 3.7. AC Response of Pressure transducer and the PSP at 420 Hz

The frequency response of the pressure-sensitive paint, in decibels, is determined by dividing the root-mean square (RMS) of the PSP by the RMS of the pressure transducer at each resonant frequency where data was collected with the equation below.

$$\text{Amplitude Ratio (dB)} = 20 * \log_{10}\left[\frac{(V_{PSP})_{RMS}}{(V_{Transducer})_{RMS}}\right] \tag{3.5}$$

The frequency response of PSP can be compared to the response of standard dynamic systems. The magnitude and phase responses of a 1st order system are given in (3.6) and (3.7).[42]

$$A_1(\omega) = \frac{1}{\sqrt{1+(\omega\tau)^2}} \tag{3.6}$$

$$\phi_1(\omega) = -\tan^{-1}(\omega\tau) \tag{3.7}$$

Similarly, response of the 2nd order system can be written as:

$$A_2(\omega) = \frac{1}{\sqrt{1+(\omega\tau)^4}} \tag{3.8}$$

$$\phi_2(\omega) = -2\tan^{-1}(\omega\tau) \tag{3.9}$$

The amplitude and phase response graph of the PSP data is shown in Figure 3.8, where the amplitude ratio in dB is calculated as in (3.5) and the phase shift is determined by using the *xcorr* function in Matlab to find the cross correlation between the PSP signal and the pressure transducer signal.

For a 1st order system, the amplitude ratio has a roll-off slope of -20 dB/decade and the phase shift levels off at -90°. For a 2nd order system, the roll-off slope should be -40 dB/decade and the phase shift should level off at -180°.[42] Using a combination of the *cftool* command in Matlab and the equations used by Winslow et al.[42], analytic functions

(Equations ((3.10) – ((3.12)) are found to adequately fit the amplitude and phase response of this model and are shown below in Figure 3.8.

$$A_{Model}(\omega) = \frac{1}{\sqrt{1+(\omega\tau)^{16}}} \tag{3.10}$$

$$\phi_{Model}(\omega) = -4\tan^{-1}(\omega\tau) - \frac{16.28}{9.413+11.14\gamma e^{2.743\gamma}} \tag{3.11}$$

Where $\omega = 2\pi f$, $\tau = 4.35\text{x}10^{-5}$s, and

$$\gamma = \left[\log\left(\omega\tau/1.215\right)^{2}\right]^{2} \tag{3.12}$$

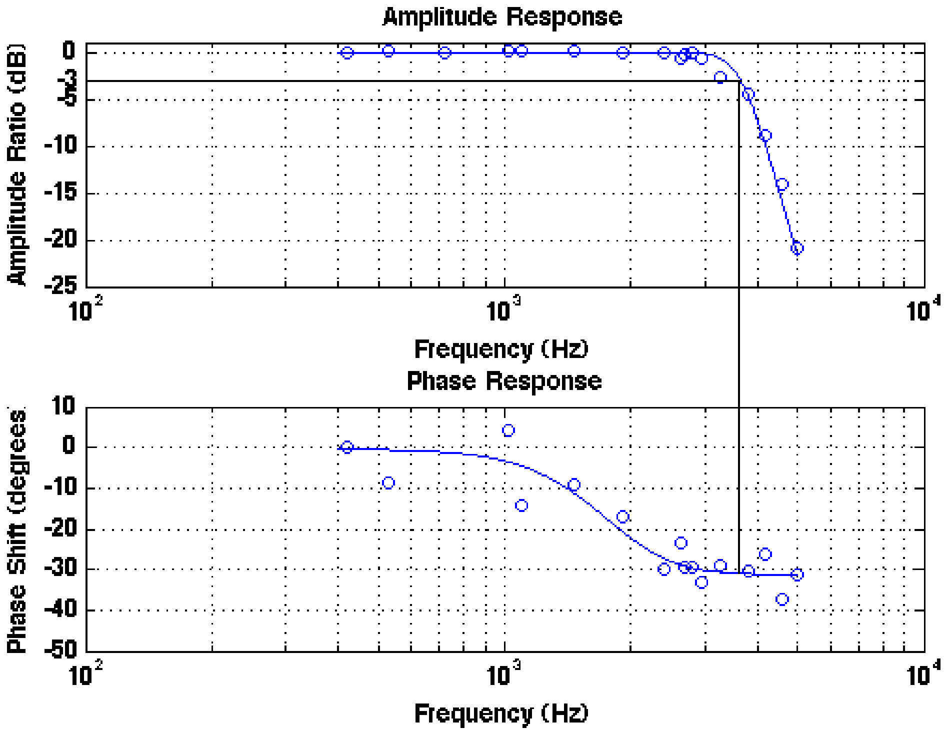

Figure 3.8. Relative Frequency Response of the PtTFPP PC-PSP Sensing Layer (30 µm)

The trend of the response is similar to what was shown by McGraw[43], however the high-frequency asymptote of the amplitude ratio is very steep, suggesting that this PSP model is that of higher order than a 2nd order system. The amplitude ratio data fits well to the 4th order system shown in (3.10), however, the phase shift seems to level off at -32° for high frequencies, which is much lower than what is expected from a higher order system. By studying the plots in Appendix A it can be seen that the phase shifts between the two signals are very small, even at high frequencies.

The "break" point of such models is defined as the frequency at which the magnitude of the voltage transfer function is reduced by $1/\sqrt{2}$, or -3 dB from its maximum value. This break point frequency indicates the location at which the luminophore's lifetime is too long to successfully resolve higher frequencies. The frequency at the break point for this system was found to be 3700 Hz, which is high enough to resolve the unsteady pressure fluctuations to be discussed in this work.

A main source of uncertainty with these measurements is photodegradation. Since the data taken at each frequency location was averaged over 200 cycles, the laser was continuously illuminating the PSP for around 15 seconds for each set of data. If photodegradation played a major role in the results, it could explain why the PSP model is that of a much higher order than results obtained by McGraw.[43] This may also lead to the possibility that the break point frequency for this paint formulation may be much higher than what was obtained in this experiment.

Chapter 4 : Experimental Setup and Data Acquisition

4.1 Background and Motivation

The present work will study the flow field around a hemispherical dome, by implementing three different PSP measurement techniques. The flow field around such a dome is complex, as reported by Vukasinovic et al.[44], where studies were conducted on the flow over a surface-mounted hemispherical shell in a wind tunnel using particle image velocimetry (PIV) at Reynolds numbers up to 700,000. Taneda was one of the first researchers to study the flow structure behind a sphere at Reynolds numbers greater than 10^4 by means of flow-visualization methods.[45] According to his results, at Reynolds numbers between 3.8×10^5 and 1×10^6 the sphere wake forms a pair of streamwise line vortices at a short distance from the streamwise axis. The vortex pair rotates slowly and randomly about that axis. Later, Sakamoto and Haniu conducted hot-wire measurements over spheres in a uniform flow to study the vortex shedding structures, and observed a progressive wave motion of the wake with alternating fluctuations, and cylindrical vortices shed periodically with this pulsation.[46]

The present study is particularly important in the development of aero-optical systems, where knowledge of the global surface pressure fluctuations can influence the design of the external optics housing in order to minimize optical distortion caused by unsteady aerodynamic phenomena. Recently, Gordeyev et al. reviewed a series of research efforts from the past few years on the study of fluid dynamics and aero-optics of hemispherical turrets.[47] Typical sources of aero-optical distortions include turbulent boundary layers, separated shear layers, and wakes. Separated shear layers are particularly destructive because of the presence of coherent vortical structures with their concomitant pressure/density wells inside them.[48] Some previous studies on such systems include flow-control methods applied on aircraft turret models[49, 50] and the characterization of the baseline flow field over a conformal-window turret.[51] Recently, studies of active control methods over a hemispherical dome model at several Mach numbers were conducted.[52] They found that the flow separation point moved upstream as Mach number increased, and a localized shock wave was found at M = 0.64, which contributed to a significant shift in the separation point to just behind the hemisphere apex.

The work presented here extends earlier experiments conducted on the study of unsteady flow over a hemispherical dome using the PSP technique.[53] In the present work, a different luminophore compound is used, and three different PSP data-acquisition techniques are implemented and compared (see Chapter 2.2 Measurement Techniques) to the study of flow over a hemispherical dome at $Re=2.4\times10^6$.

4.2 Experimental Setup

Wind Tunnel

The hemispherical dome experiment was conducted in the Air Force Research Laboratory's Trisonic Gasdynamics Facility (TGF), a closed-circuit wind tunnel with a test section measuring 2 feet high by 2 feet wide. In this facility, the Mach number can be varied from 0.3 to 3.0 through the use of guide vanes in the compressor at subsonic speeds, and fixed discrete nozzle blocks at supersonic speeds. The characteristic that makes this wind tunnel ideal for PSP testing is the capability for the user to adjust the tunnel temperature and pressure independently. This is extremely useful for an *a priori* calibration of the PSP formulation, which was accomplished in the present work by varying the tunnel pressure from 12.0 kPa up to 101.4 kPa to obtain the PSP surface intensity values over the dome at seven different pressures.

Hemispherical Dome

The hemispherical dome used in this work, shown in Figure 4.1, was provided by the U.S. Air Force Research Laboratory (AFRL). The model measures 0.254 meter in diameter and is constructed primarily of an epoxy material, with a small metallic disk located at the apex. An array of 13 pressure taps located along the centerline of the model was used for performing an *in situ* calibration of the PSP, as well as to provide a benchmark for accuracy of the PSP data. Kulite pressure transducers were strategically installed just aft of the dome apex to obtain the fluctuating pressure signature of the unsteady separated shear layer. Figure 4.2 shows a schematic of the hemispherical dome as well as the location of the pressure taps and Kulite pressure transducers. Figure 4.3 shows a CAD model of the hemispherical dome mounted on the splitter plate. The base of the hemispherical dome is approximately 5 cm away from the wind tunnel wall.

Figure 4.1 Hemispherical Dome

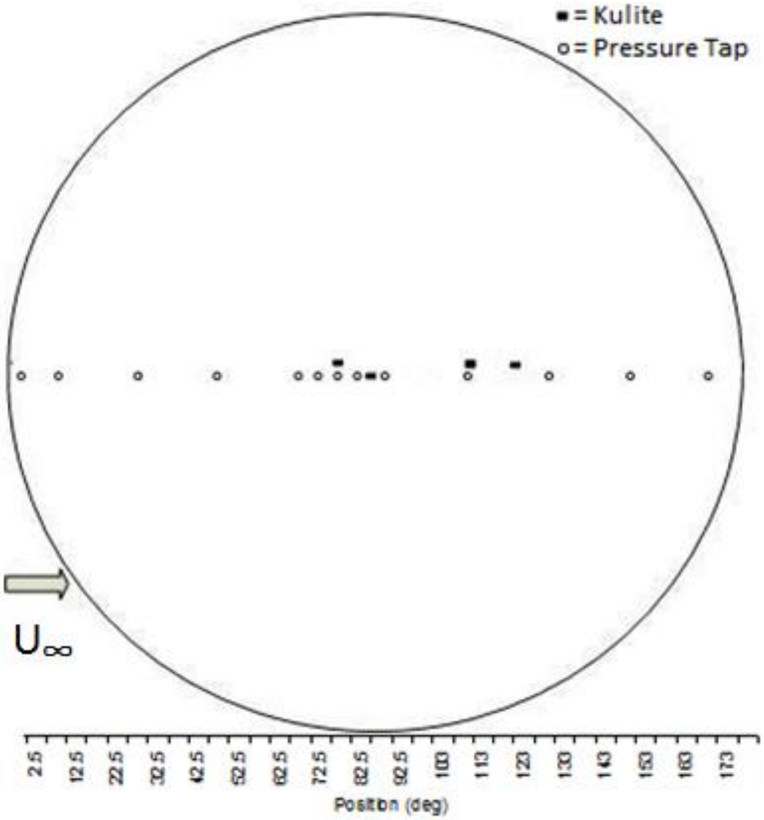

Figure 4.2 Pressure Instrumentation Locations

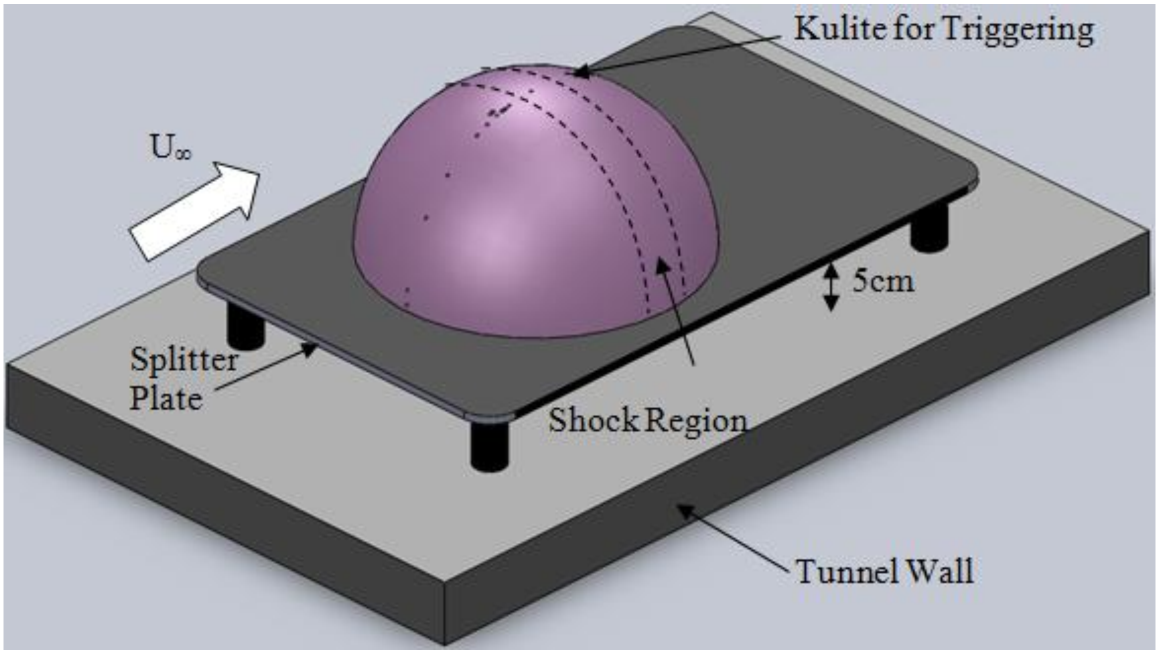

Figure 4.3 Installation of Hemispherical Dome in Test Section

4.3 Instrumentation

Phase-Averaged Technique

The setup for the phase-averaged data acquisition method is shown in Figure 4.4. The hemispherical dome was painted with a porous polymer/ceramic binder layer and over-sprayed with platinum tetra (pentafluoro-phenyl) porphyrin (PtTFPP) complex as the luminophore. Details on the preparation of polymer/ceramic PSP are provided by Gregory et al.[3] and discussed in the earlier sections of this thesis. This PSP formulation has a peak absorbance and emission spectra at λ=388 nm and λ=650 nm, respectively.[6] The lifetime of PtTFPP is about 10 μs at the pressure condition studied (~ 72 kPa). This lifetime is much longer than that of the bathophen ruthenium luminophore (0.13 μs), which has conventionally been used for fast-responding PSP.[3] Despite its longer lifetime, PtTFPP is much more sensitive to smaller pressure changes and is still suitable for experiments with pressure oscillations on the order of one kilohertz.

Two violet LED arrays (wavelength 405 nm) illuminated the front and aft portions of the model. A Cooke Corp. PCO.1600 CCD camera with 1200x1600-pixel resolution imaged the surface luminescence distribution on the model. A 590-nm long-pass optical filter (Schott Glass OG590) was fitted in front of the camera lens to filter out the excitation light, allowing only the emitted light to be captured. Since an intensity ratio between the wind-on and wind-off images must be obtained to acquire the pressure data, the two images must be aligned to avoid significant errors. During operation of the wind tunnel, the vibration of the side walls posed a threat to proper alignment of the camera between images. By securing the CCD camera and LED units to the wind tunnel with three aluminum trusses, the camera was able to shift with the wind tunnel motion while images were acquired.

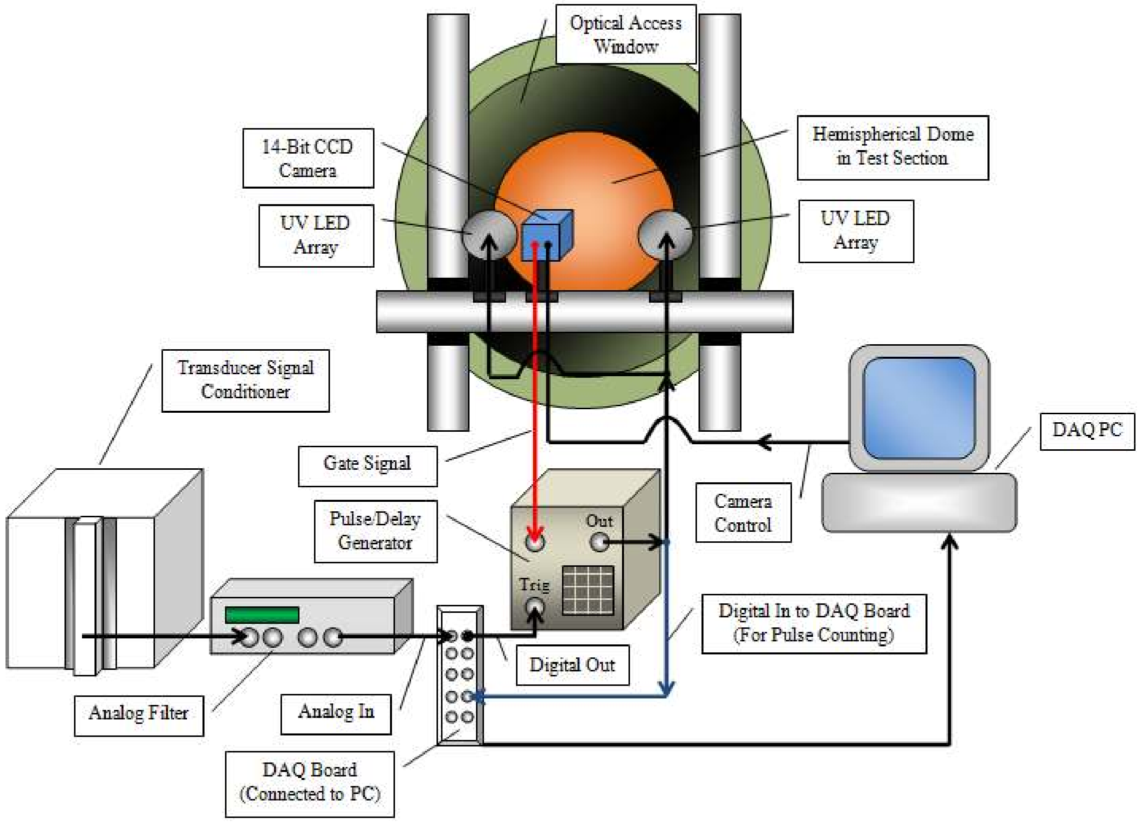

Figure 4.4 Phase-averaged Data Acquisition System

The unsteady pressure signals from the Kulite transducers were acquired digitally using a National Instruments SCXI-1000 signal conditioner. In parallel to this process, one of the unconditioned (analog) transducer signals was selected for triggering and phase-locking the PSP data acquisition. A Krohn-Hite Model 3364 analog filter was used to amplify and filter the trigger signal. For the test condition at M= 0.6 and P_0= 71.84 kPa, a tight 8th-order band-pass filter with high-pass cutoff frequency of 390 Hz and low-pass cutoff of 410 Hz, was used to lock onto the fundamental shear layer frequency of 400 Hz. In order to capture the flow field at given points in the shear layer oscillation cycle, the LED arrays were required to pulse at the same frequency as the fluctuations.

Thus, the excitation from the LED array was phase-locked to the predominant shear layer frequency measured by the pressure transducer. Triggering, pulse-delaying, and camera settings were all controlled using a LabVIEW data acquisition program with input signals from a National Instruments 6251 DAQ board. A pulse/delay generator (Berkeley Nucleonics model 575) was used to gate the LED pulses with the camera exposure signal such that the LEDs did not pulse while the camera shutter was closed. This reduced the effects of photo-degradation inherent with the luminophore molecules.

A significant problem in the phase averaging technique was encountered when applied to this flow field. Historical implementations of the phase-averaging technique have involved flow fields with a fairly repeatable (periodic) waveform, with frequency and amplitude that were constant. In the frequency domain, this type of signal would appear as a tall, narrow peak on a power spectrum. In contrast to those benign, controllable cases, the current flow situation exhibited much more random fluctuations in the shedding frequency and amplitude. Inevitably, when a phase-averaging technique is locked onto such a signal, the number of cycles occurring within a given camera exposure (fixed period of time) will vary from image-to-image due to frequency jitter. Since the instrumentation system produces one light pulse for every cycle, the total amount of light illumination during a single camera exposure will vary due to frequency jitter. Furthermore, this effect is exacerbated when the phase-averaged delay is set to a value late in the cycle. Under this condition, delays of the instantaneous period beyond the mean period, along with a finite residence time for re-arming the triggering mechanism, causes a significant number of pulses to be missed (over 50%). The end result of these two phenomena is that many light pulses can be missed in a given image, causing non-repeatable illumination of the model. The variation of light intensity can be quite significant, so much so that the errors due to light variation overwhelm the indicated pressure signal.

In order to alleviate the effects of these illumination variations, the total light intensity for each image was monitored and recorded. A digital pulse counter was used to monitor the number of triggers sent to the light sources. The camera was set to capture and average four images, each with an exposure time of 250 ms, while the LED arrays excited the PSP at a rate of 400 Hz. This combination indicates that the optimum number of pulses needed to fill the capacity of the CCD sensor for each image is 100. The total number of light pulses for a given image at each delay was not allowed to vary by more than 5% of the total number of pulses received by the first image. After data acquisition, the overall intensity of each image was normalized to the intensity of the first captured image by the number of light pulses counted for a particular image. A comparison of the intensity level before and after the correction is shown in Figure 4.5, where the uncorrected intensity level fluctuated about 0.6% throughout the cycle, but at the last delay, the intensity lowered significantly by 8%. After the correction has been applied, the intensity level variations from image to image are less than 0.2%, giving much better results than the uncorrected data.

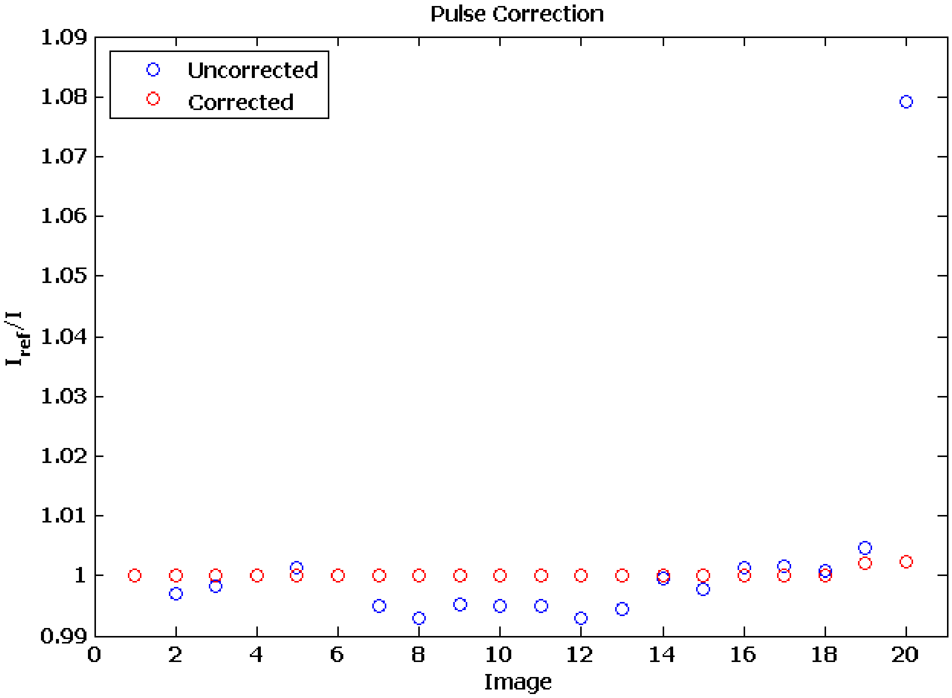

Figure 4.5 Intensity Variations Between Phase-averaged Images

The test conditions presented in this work are at Mach 0.6 with total pressures of 71.84 kPa, where the shear layer frequency was measured by a pressure transducer to be 400 Hz. The recorded Reynolds number, based on dome diameter, was 2.41 million. Twenty delay steps were used, with each delay step taken as 5% of the oscillation period.

Real-time Technique

While the phase-averaging technique can provide good quality time-averaged data showing the bulk of the varying pressure gradient, certain aperiodic characteristics may be "averaged-out" and may not be present in the final results. One approach to this problem is imaging with high-speed cameras and continuous illumination to obtain unaveraged surface pressure data in realtime. The setup for this technique is shown in Figure 4.6.

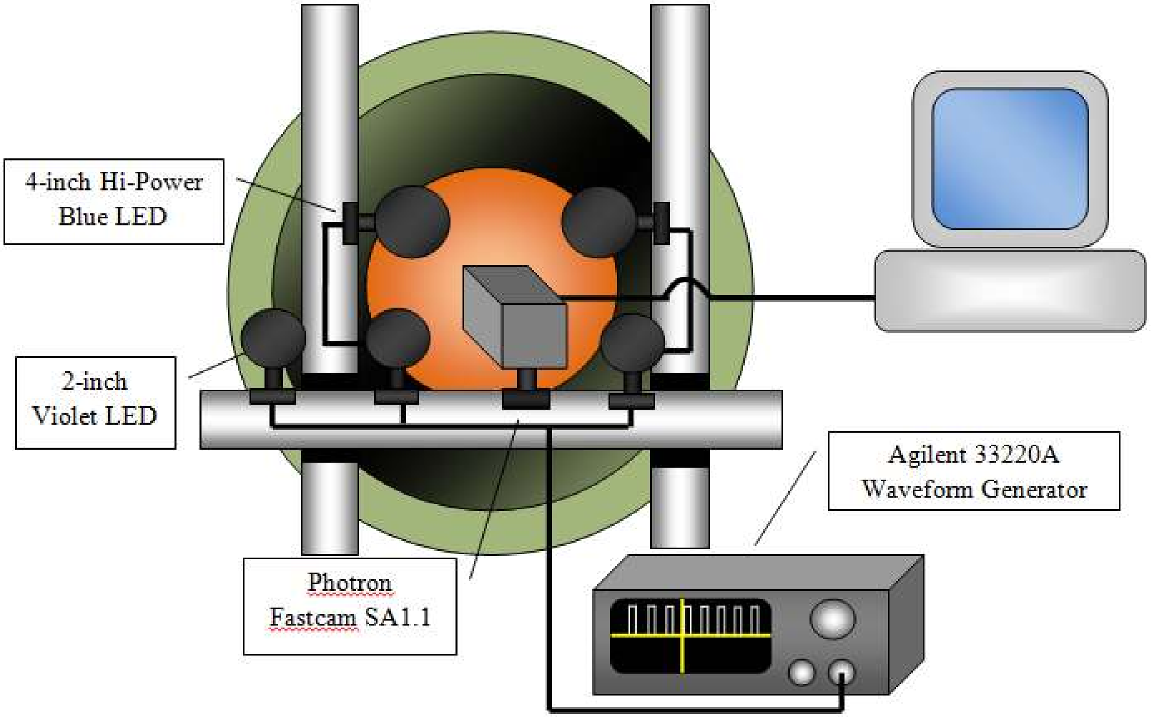

Figure 4.6 Real-time Data Acquisition System

The luminescence on the hemispherical dome model was observed through the optics window on the wind tunnel. The PSP on the model was illuminated continuously with five LED arrays to provide sufficient light for lowering the noise level of the high-speed camera due to the fast shutter speed. Three of the excitation light sources were 2-inch violet LED arrays with 405 nm emission for optimum excitation of the PtTFPP luminophore, and the other two were 4-inch blue LED arrays with 473 nm emission to provide high-power uniform illumination of the model. All five LED lamps were driven by a waveform generator that provided a continuous 5-Volt signal to maintain illumination. The luminescence on the model was captured by a thermoelectrically cooled, high-speed color camera with 12-bit depth (Photron Fastcam SA1.1) through an optical high-pass filter. The camera system has a variable frame rate from 60 fps with 1024 x 1024 pixels up to 675 kHz with 64 x 16 pixels. All camera settings can be adjusted by using the provided software to obtain an optimum combination of frame rate and resolution for the given flow field to be measured. For the current work, the imaging of the surface pressure distribution was performed at a frame rate of 10 kHz with an image resolution of 768 x 768 pixels, which was enough for capturing the 400 Hz fundamental frequency of the shear layer over the test model.

Lifetime Technique

The lifetime-based single-shot technique is an approach to dealing with some of the disadvantages of the previous two techniques, such as eliminating the need to acquire several excitation exposures just to obtain one image for the phase-averaging technique, or the high noise level and low spatial resolution of the real-time method. The setup for the single-shot method is shown in Figure 4.7.

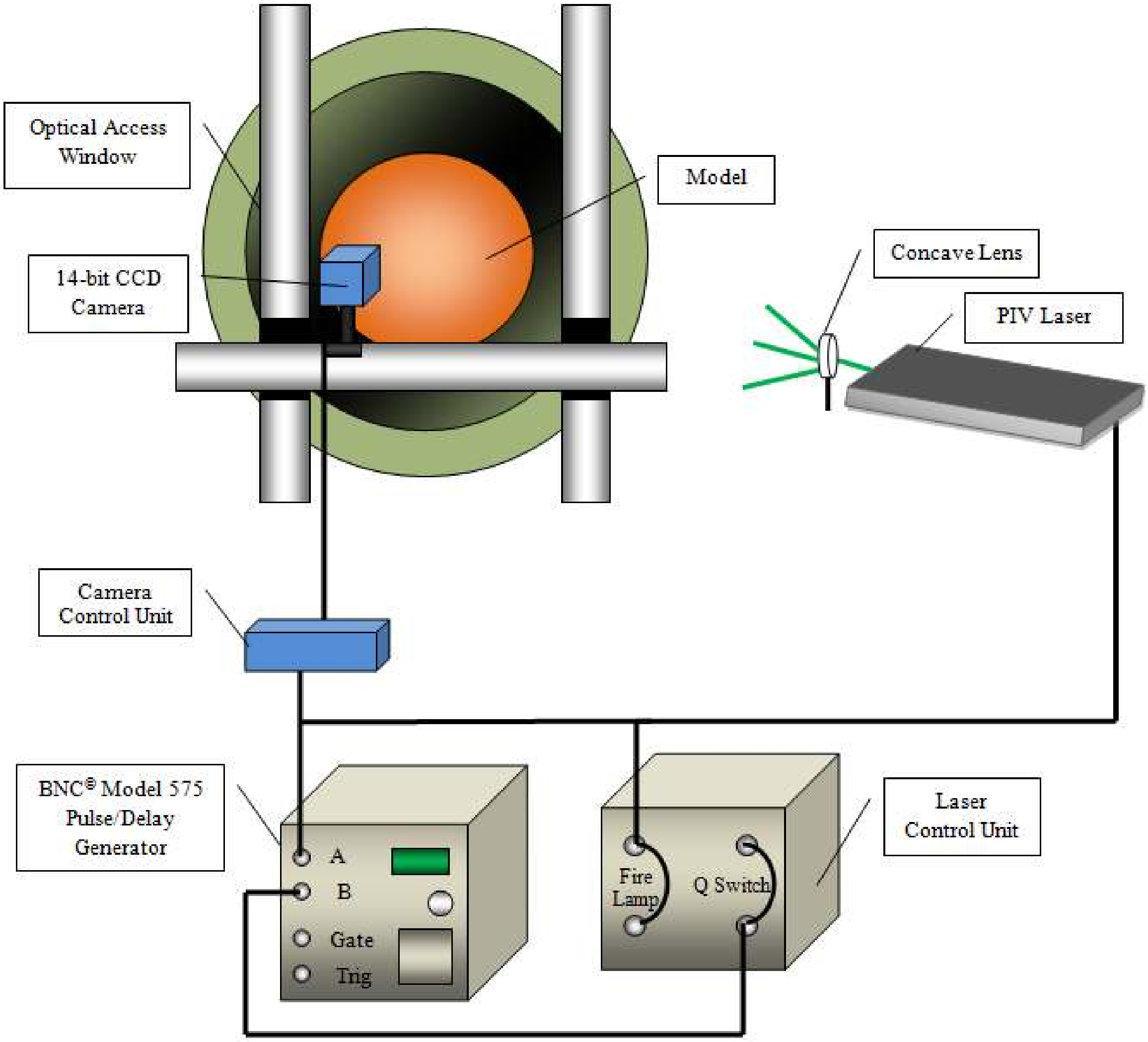

Figure 4.7 Lifetime Data Acquisition System

In the lifetime-based system, the illumination source for the PSP is provided by a high-power New Wave Solo 200 XT 532-nm PIV laser that emits 200 mJ per pulse, thus compensating for the fast shutter speeds and increasing the signal-to-noise ratio. The laser was placed approximately 5 meters away from the optical viewing glass of the wind tunnel. The laser light is expanded using a negative lens to create a laser sheet, providing uniform illumination of the test model.

A 14-bit monochrome charge-coupled-device (CCD) camera (PCO.1600) was used to capture the paint luminescent intensity. The camera was mounted on the wind tunnel with a slight tilt as compared to the mounting position for the phase-averaging technique in order to avoid laser reflection from the optical access window of the wind tunnel. To capture the luminescent signal in a two-gated mode, the CCD camera is set to "double shutter" mode using the Camware software. In this mode the camera acquires one image for a specified time period, saves it to a buffer, and then takes another exposure immediately after. These two images provide the two luminescent intensity images used in the lifetime data. The camera specification for this double shutter mode is schematically shown below in Figure 4.8, where t_{exp1} denotes the first exposure time, which can be adjusted by the user to any value over 0.5 μs. The second exposure, denoted by t_{exp2}, cannot be adjusted and is determined by the readout time of the first image. The interframing time, t_{itf}, is the time for the camera to transition from the first exposure to the second exposure, which is 180 ns for the particular camera used in this experiment.[54]

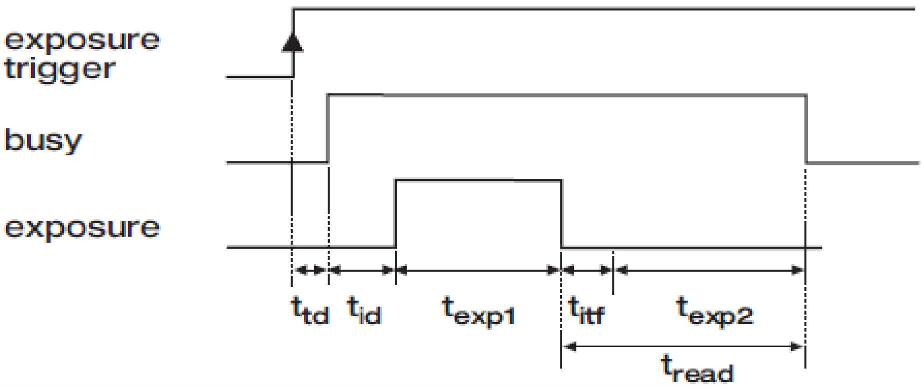

Figure 4.8 PCO.1600 Output Signals for Double Shutter Mode[54]

Although the fundamental shear layer frequency of interest in this experiment was 400 Hz, the PIV laser has an upper-limit repetition rate of 15 Hz and the CCD camera is limited to 30 frames per second. Therefore, the timing between the camera and laser systems was synchronized using a pulse/delay generator that provided a 5 Hz TTL signal to both the laser and the camera. Figure 4.9 shows a schematic of the timing signals specified for this experiment. The pulse/delay generator was used to set a delay of 250 μs between the Q-switch activation and the flash-lamp firing. Besides the camera trigger acknowledgement delay of 0.2 μs, an intrinsic shutter opening delay of 5 μs was set such that the camera shutter does not open until this time has passed. The optimum exposure for Gate 1 was found to be 247.1 μs after comparing light output levels of images obtained for both gates at different exposure values.

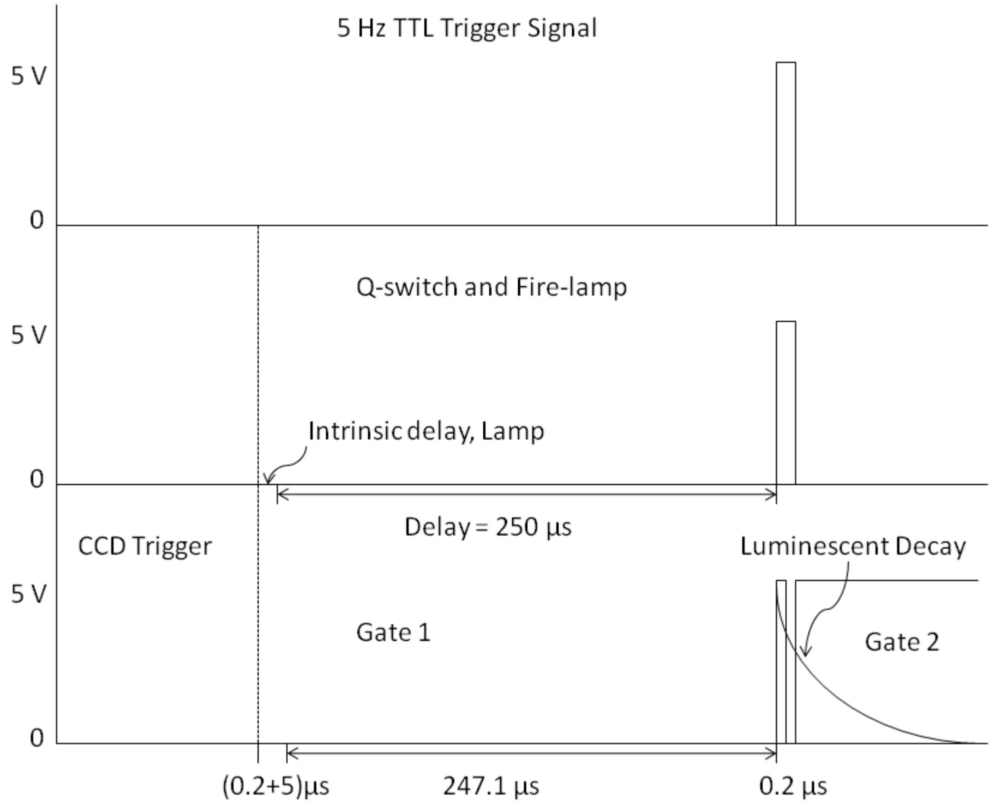

Figure 4.9 Timing Diagram of Lifetime Setup

For the lifetime method, the set of wind-on images was acquired when the wind tunnel had stabilized the experimental conditions. Ideally, all the pressure information could be obtained from a ratio of the two gated images. However, it has been found that a major error in the lifetime-based pressure measurements is due to pixel-to-pixel variations of the paint calibration that can be reduced by taking a wind-off ratio.[11] The two gatedwind-off images were acquired after the airflow had stopped in the wind tunnel.

Chapter 5 : Results

5.1 Phase-averaging Method

Data Reduction

For the phase-averaging method, the full-field images acquired from the CCD camera were used to obtain the intensity ratio by dividing the reference image intensity by the phase-averaged wind-on image intensities. The pressure signals were then converted to a pressure ratio by dividing the static pressure by the total pressure. The measured intensity ratio was converted to pressure ratio through an *a priori* calibration followed by an *in situ* adjustment. The *a priori* calibration was conducted directly on the model installed in the wind tunnel. A separate calibration for each pixel was determined by acquiring images of the model at various static pressure conditions (wind off) inside the tunnel, ranging from 12.0 kPa up to 101.4 kPa. This pixel-by-pixel calibration was performed to counteract errors due to spatial variation in calibration due to extremely oblique viewing angles. Even though PSP calibration is theoretically independent of viewing angle, in practice the calibration can change when a model is viewed from oblique angles. When Bencic studied this behavior with PSP applied to a jet engine exhaust nozzle, he found that the calibration remained constant (within 1%) at angles up to 70° from a normal viewing angle. Beyond this angle, however, variations in the calibration coefficients reached 3% at oblique angles of 80° and higher.[55] Since imaging of the hemispherical dome inherently involves oblique viewing of the model edges, the pixel-by-pixel calibration of the model in the wind tunnel was performed to counteract these errors.

The calibration data was fit to the Freundlich model, which is often used for porous paints,

$$\frac{I_{ref}}{I} = A(T) + B(T)\left(\frac{P}{P_{ref}}\right)^{\gamma} \tag{5.1}$$

where I is the intensity, P is the static pressure, *ref* indicates the reference intensity and pressure values obtained during wind-off conditions, and $A(T)$, $B(T)$, and γ are temperature-dependent constants obtained from the calibration process. Once the reference pressure is known, the static pressure at a given point on the painted surface can be obtained from the corresponding ratio of intensities.

Finally, an *in situ* adjustment was applied to relate the intensity ratio to the pressure ratio, measured by the pressure taps, for each pixel in the image. The adjustment consists of an amplitude and slope shift of the PSP data by using two of the pressure taps, namely at the 32° and 72.5° locations. Figure 5.1 shows a comparison of the PSP data before and after the *in situ* adjustments were applied. As can be seen from the figure, the PSP data correlated very well with the pressure tap data after the adjustments were made. The error past the 90° location will be discussed further in the following sections.

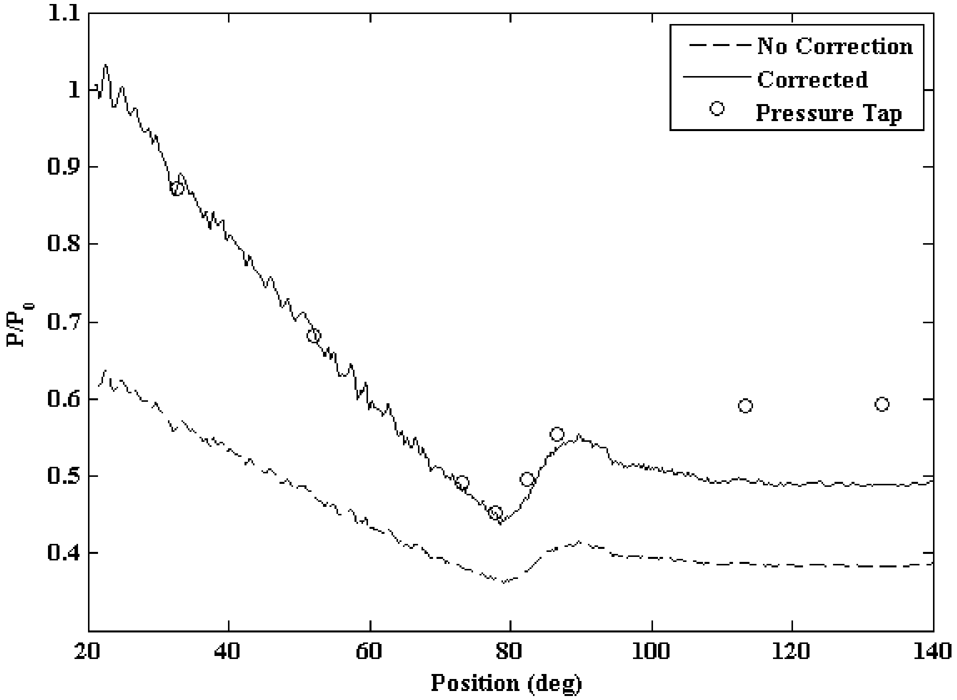

Figure 5.1 Pressure-sensitive Paint Data Before and After *in situ* Adjustment

Full-field Unsteady Data

The unsteady PSP results for the test condition at M=0.6, P_0=71.84 kPa are presented in the sequence of images in Figure 5.2, where the arrows denote the shock front as determined by the sudden increase in pressure. The image times are fractions of the shear layer oscillation period, T_0, which was 0.25 ms. The data were captured by triggering the excitation source from the rising edge of the reference signal. Several characteristics of the indicated surface pressure distribution can be observed from Figure 5.2. A circle-shaped intensity change is observed for all the images, which is believed to have been caused by the circular aluminum disk located at the dome apex. Since a change in the substrate material can cause a change in the local heat flux, and thus surface temperature, the PSP (which is also temperature sensitive) will react to this temperature change with a noticeably different light emission signature. This explanation has been verified by a separate temperature-sensitive paint (TSP) test using a Ruthenium-based TSP formula and the same data acquisition techniques as that for the PSP. The results in Figure 5.3 show a 3 Kelvin temperature difference between forward and aft portions of the model. Therefore, the region bounded by the circular shape should be disregarded from the rest of the data.

A shock oscillation can be clearly observed in the cross-sectional data, shown in Figure 5.4, taken along a profile on the model indicated by the red line. Figure 5.5 shows a close up of the cross-sectional data from the previous figure, focusing in the shock oscillation region. A time history of the signal from one point on the PSP surface, normalized by an adjacent tap at 113°, is shown in Figure 5.6. The CAD model shown in Figure 4.3 shows the region in which the shock oscillates, and the Kulite pressure transducer used for triggering.

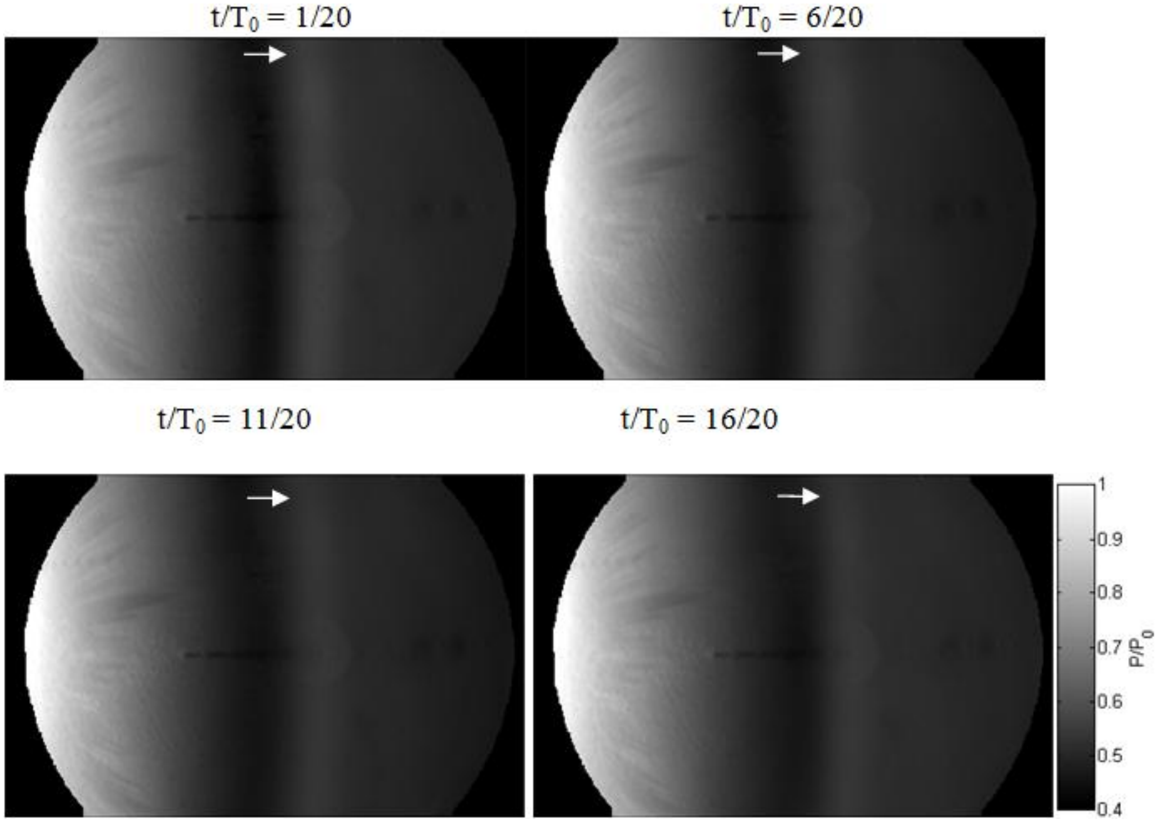

$t/T_0 = 1/20$ $t/T_0 = 6/20$ $t/T_0 = 11/20$ $t/T_0 = 16/20$

Figure 5.2 Unsteady Phase-averaged PSP data at Mach 0.6 (P_0=71.84 kPa, T_0=0.25 ms)

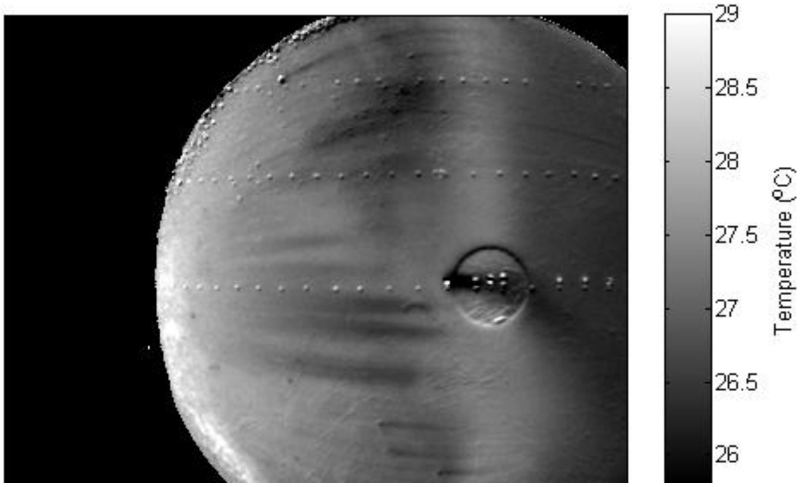

Figure 5.3 Unsteady Phase-averaged TSP data at Mach 0.6

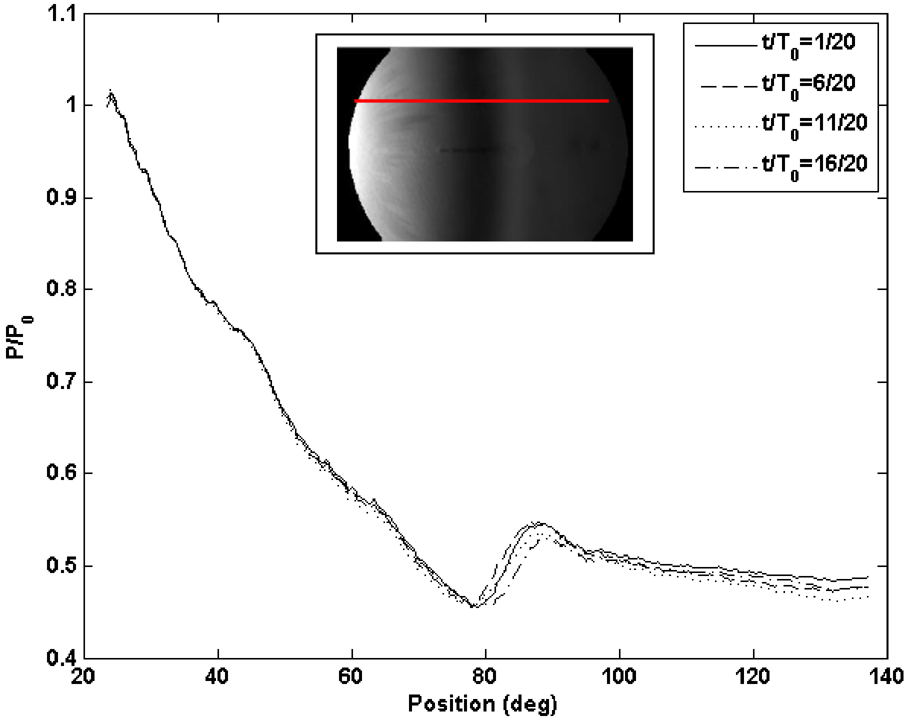

Figure 5.4 Cross-sectional PSP Data at Mach 0.6 (P_0=71.84 kPa, T_0=0.25 ms)

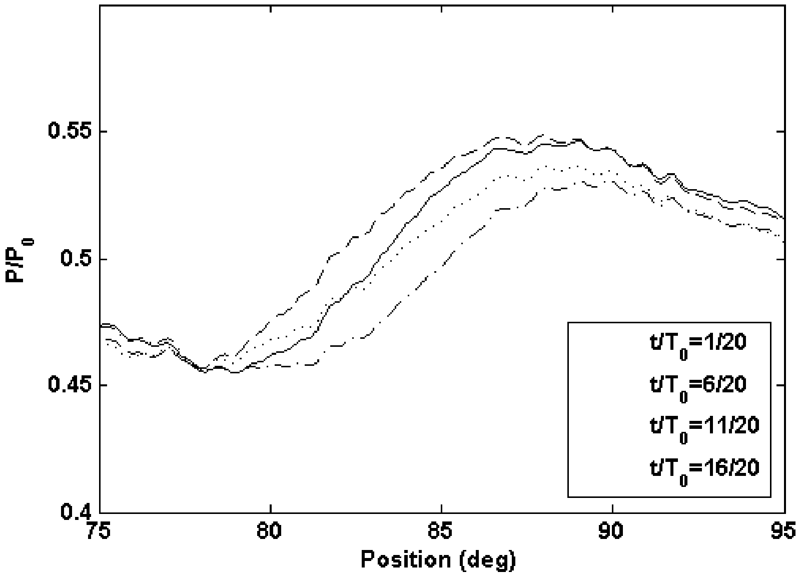

Figure 5.5 Close-up of Cross-sectional PSP Data (P_0=71.84 kPa, T_0=0.25 ms)

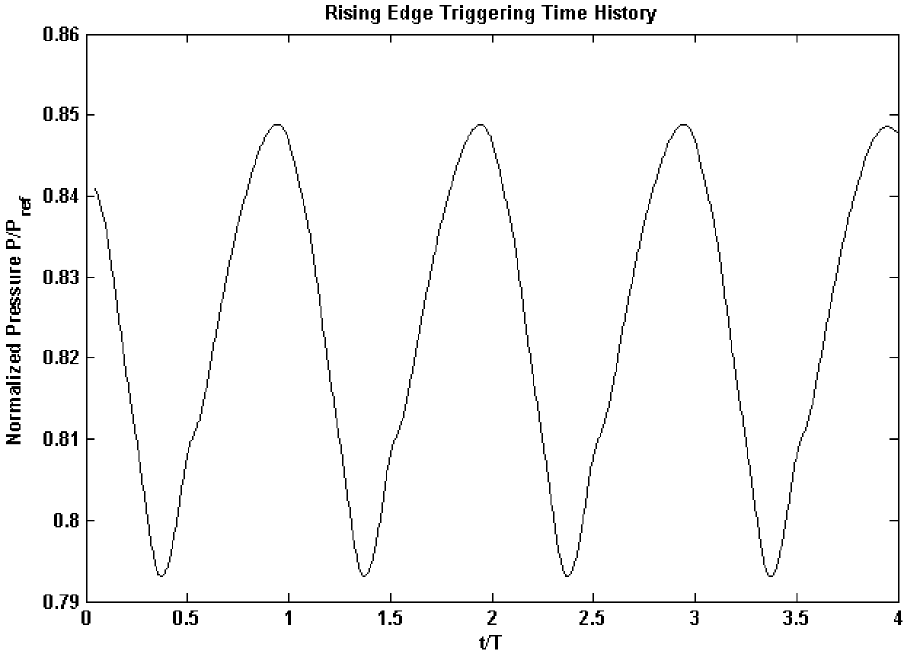

Figure 5.6 Time History of Rising-edge Triggering

A comparison between the PSP data and the actual pressure values at corresponding azimuthal locations, obtained by the pressure taps mounted along the center of the model, is shown in Figure 5.7. From the image, it can be seen that the PSP data correlates very well with the pressure tap data at the front and mid-sections of the model, but deviates near the aft section. This is due to the PSP's reaction to the unequal temperatures between the front and aft sections of the model caused by the flow separation shown in Figure 5.3.

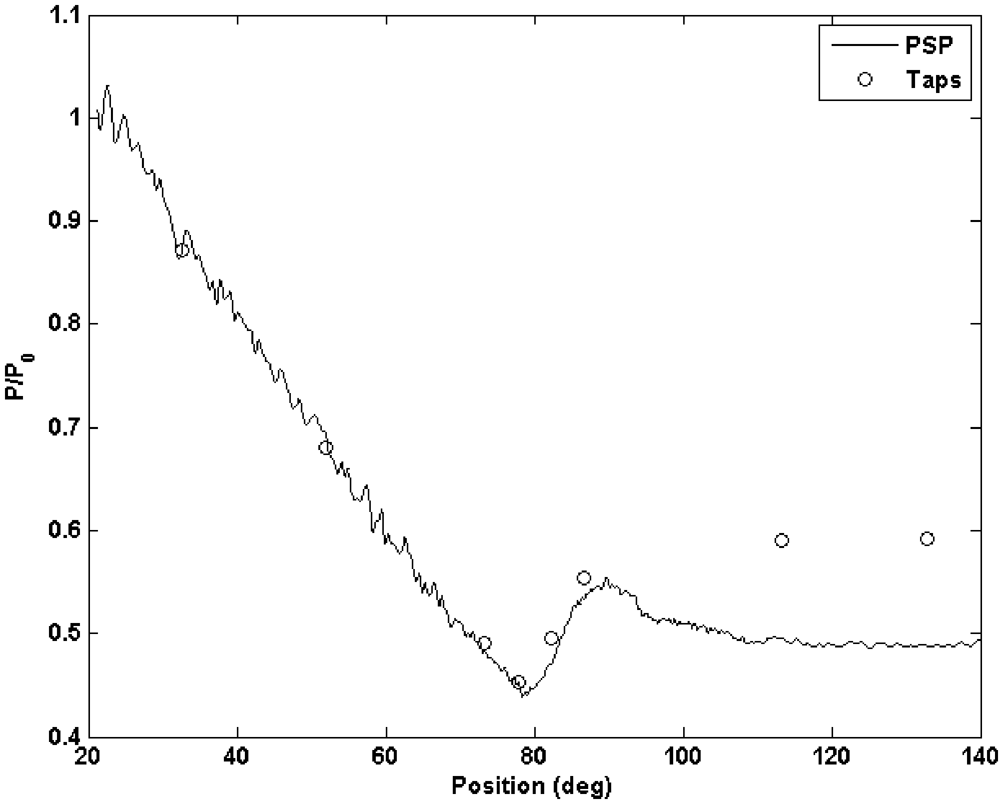

Figure 5.7 Comparison of PSP and Pressure Tap Data for Phase-Averaging Method

Dependability of Phase-Averaging Technique

The integrity of the phase-averaging technique depends on the accuracy of how well the illumination source locks onto the unsteady signal. As mentioned before, as the delay is stepped closer to the end of the period, triggering events will be missed due to the unsteadiness of the waveform and inadequate rearming speed of the hardware. One way to verify the dependability of the phase-averaged data is from acquiring sets of data by locking the excitation source to both the rising and falling edge of the reference signal. If events are triggered correctly for all delay increments, the two sets of data will produce data showing the shock oscillation to be 180° out of phase. A comparison between the rising-edge and falling-edge triggering time histories is shown in Figure 5.8, where a 180° phase-shift is applied to the falling-edge time history, and both sets of data are normalized by the pressure tap at 113° location. Figure 5.9 shows the error between the falling-edge and rising data, which is no more than 2% of the normalized pressure. The two plots agree well with each other, validating the accuracy of the phase-averaging technique.

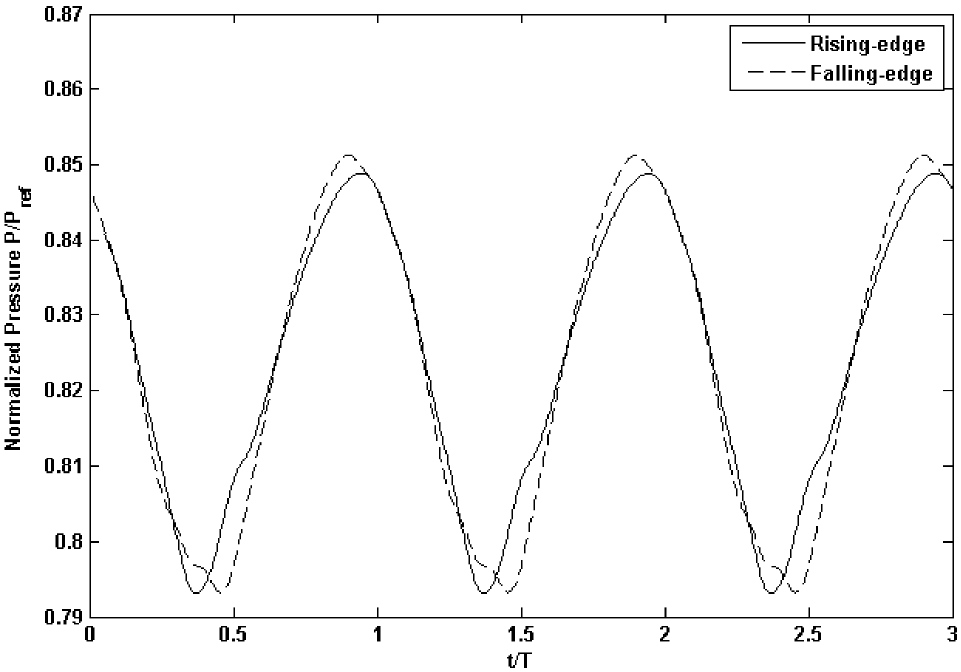

Figure 5.8 Falling-edge and Rising-edge Triggering Comparison

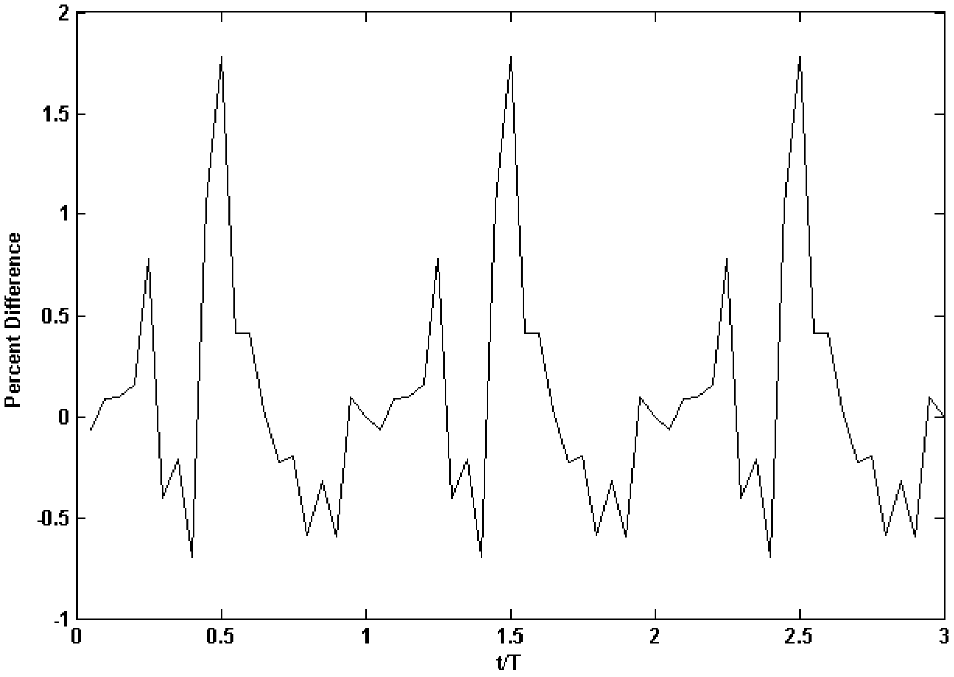

Figure 5.9 Difference Between Rising-edge and Falling-edge Data

Differential Pressure Results

The phase-averaging technique can be used to present data showing solely dynamic pressure changes, neglecting the mean pressure gradients and essentially producing an AC-coupled representation of differential pressure. Such a technique has been implemented in the past to counter the effects of photodegradation of PSP.[56, 21,43] PSP requires a reference image in order to remove the effects of nonuniform illumination, paint thickness, etc. A wind-off reference image is most often used; however, errors can arise when photodegradation or temperature changes take place between the wind-on and wind-off reference conditions. The AC-coupled method involves one minor change in the acquisition of the reference image: instead of taking a wind-off reference, an average of all 20 phase-delayed, wind-on images is used as the reference instead. This difference provides only the pressure fluctuations, effectively removing the mean pressure distribution. The model is typically in thermal equilibrium during the wind-on conditions, so the temperature distribution will not vary during wind-on data acquisition. In contrast, significant differences in the surface temperature arise between the wind-on and wind-off reference conditions, due to the cessation of convective heat transfer at wind-off. Thus, the AC-coupled method removes the temperature and photodegradation errors by minimizing erroneous changes in intensity between the wind-on and reference images. The sequence of images shown in Figure 5.10 illustrates the results of this concept. From the sequence of images, the region over which the shock oscillates can be clearly seen, without the distraction of other pressure gradients. Comparing the results in Figure 5.10 to those in Figure 5.2, the differential pressure method readily depicts pressure changes near the rear of the model that may indicate the interaction of the separated shear layer with the model surface, whereas this is not easily visible in the conventional data reduction method.

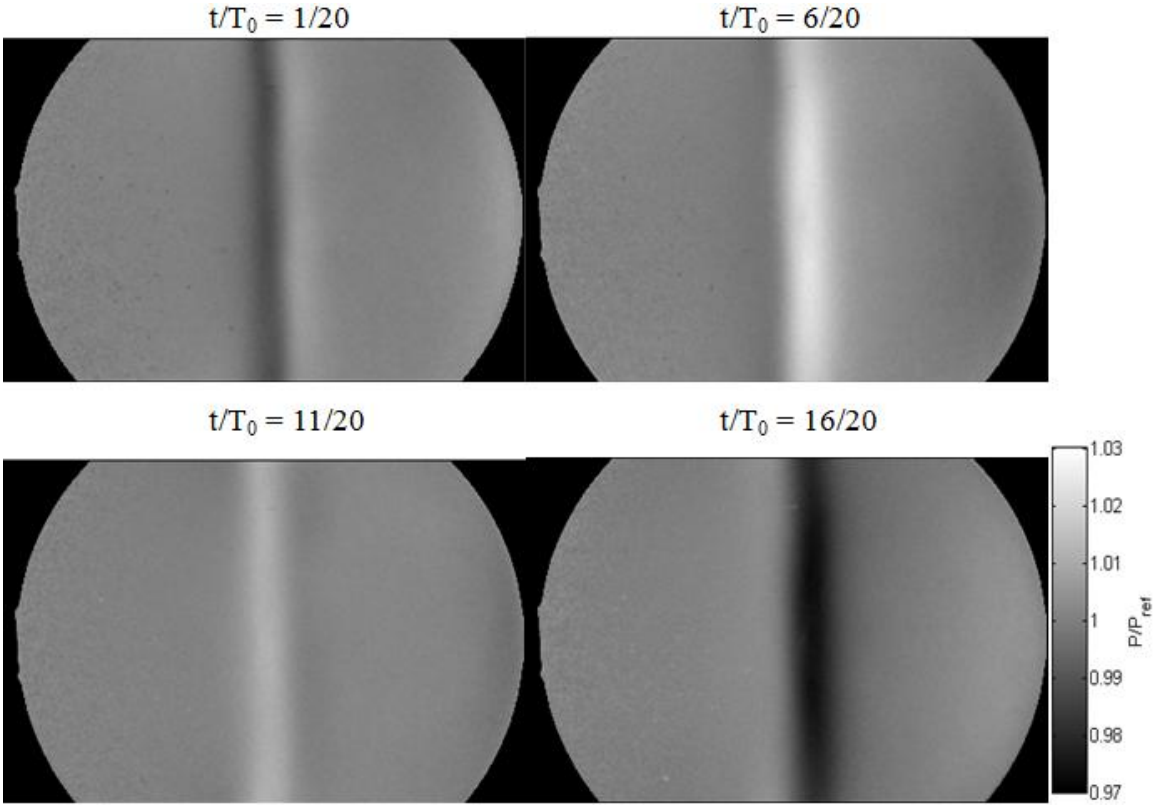

Figure 5.10 AC-coupled Representation of Pressure Differential on Model

5.2 Real-time Method

Data Reduction

The data reduction process for the real-time method is essentially the same as the phase-averaging method. Two PSP luminescent images were captured at the wind-on condition and at the wind-off condition. A dark image without luminescence was subtracted from those two images to eliminate dark current noise. The intensity ratio of the wind-off to wind-on images was converted to pressure data through an *a priori* calibration followed by an *in situ* adjustment. These calibrations were done for each individual pixel in the images to counteract any errors caused by spatial variations in the calibration data due to extremely oblique viewing angles. The calibration data is then fitted to the Freundlich model mentioned in (5.1).

Unlike the monochrome 14-bit CCD camera used in the phase-averaging technique, the camera used for this technique was a 12-bit color camera, so additional steps were taken to correct for the noise caused by the color Bayer-matrix camera sensor. According to Covington, most digital cameras sense brightness and color by combining data from the separate red, green, and blue pixels.[57] There are more green pixels than red and blue because the human eye is more sensitive to the fine details in the middle part of the light spectrum. This color matrix causes noise in the data since the RGB components of each pixel are generated by interpolating from adjacent neighbor pixels, but a long-pass filter placed in front of the camera lens only allows the camera to see color in the red spectrum. Therefore, the long-pass filter does not allow the camera to gather the necessary information from the blue and green pixels. When processing the images from the color high-speed camera, it was found that some noise may be minimized by removing the green and blue pixels from the image, but this reduces the image resolution even further.

Full-field Unsteady Data

The unsteady PSP results for the test condition at M=0.6, P_0=71.84 kPa are presented in the sequence of images in Figure 5.11. Although a few thousand images were acquired for the test condition, using the framerate of the camera, the images corresponding to the same four instances within the oscillation period for the phase-averaging technique are shown below. Like the phase-averaging technique, a circle-shaped intensity change can be observed for all the images. Since this intensity change is caused by temperature variations due to a change in the substrate material, it can be ignored in the data.

The first thing to be noted in these results is that there is a fair amount of noise compared to the data obtained in Figure 5.2. The noise can be attributed mostly to the shot noise of the camera. For the phase-averaged pressure measurements, the signal-to-noise ratio can be improved by averaging a series of images taken at the same conditions. However, it is impossible to entirely capture all the surface pressure variations of a truly unsteady (asymmetric and aperiodic) flow field, such as the present test case.

Despite the higher noise level and the lower spatial resolution in the data compared to the phase-averaging technique, much meaningful information about the flow features over the surface of the test model can be obtained. The real-time method has the ability to capture pressure variations in the flow field that are "averaged out" by the phase-averaging method. From the series of images in Figure 5.11, some very complicated interactions in the shock structure can be observed. The shock structure, which appeared to only oscillate in a planar manner along one direction over the model in Figure 5.2, also has wave-like oscillations in the spanwise direction.

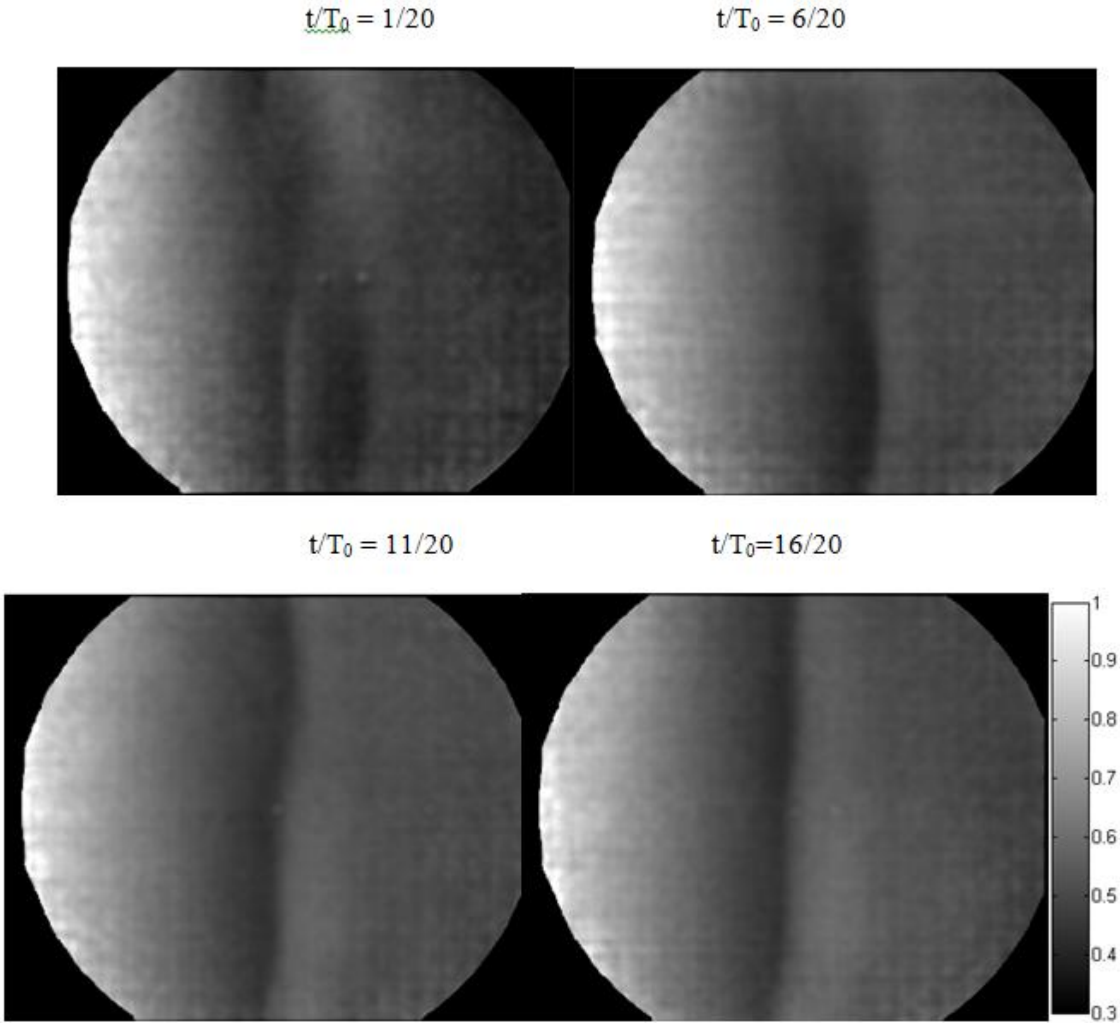

Figure 5.11 Unsteady Real-time PSP data at Mach 0.6 (P_{ref} =71.84 kPa, T_0=0.25 ms)

A comparison between the PSP data and the actual pressure values at corresponding azimuthal locations, obtained by the pressure taps mounted along the center of the model for the real-time method, is shown in Figure 5.12. Like the phase-averaged method, it can be seen that the PSP data correlates very well with the pressure tap data at the front and mid-sections of the model, but deviates near the aft section due to the PSP's response to the temperature gradient. From this image, the noisiness of the data can also be observed, as there are far more fluctuations in the PSP profile compared to Figure 5.7.

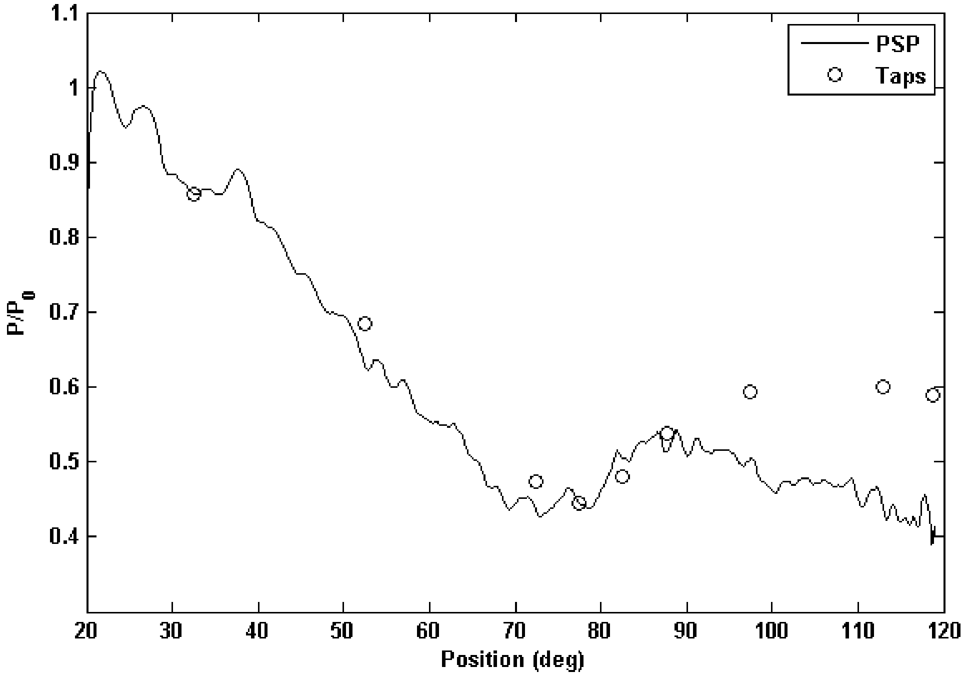

Figure 5.12 Comparison of PSP and Pressure Tap Data for Real-time Method

5.3 Life-time Method

Data Reduction

The images acquired at both gates for the wind-on and wind-off conditions all contain both the paint luminescence data and dark noise data, so a dark image was subtracted from all of the acquired images. After the correction for the dark noise, a ratio of the two gates at both the wind-on and wind-off conditions was performed. The reference signal (Gate 1) is divided by the pressure signal (Gate 2). Before applying the *a priori* pixel-by-pixel pressure calibration, a ratio of ratios (5.2) is taken to correct for any non-uniformities. Next, the ratio of the ratioed luminescent intensities around the pressure taps was extracted. Finally, an *in situ* adjustment was applied, and the PSP images were converted to pressure values.

$$\frac{\left(G_2 / G_1 \right)_{ref}}{\left(G_2 / G_1 \right)} = A(T) + B(T)\left(\frac{P}{P_{ref}} \right)^{\gamma} \tag{5.2}$$

Full-field Unsteady Data

The unsteady PSP results for the test condition at M=0.6, P_0=71.84 kPa using the lifetime-based single-shot method are shown in the series of images in Figure 5.13. The viewing angle for this test was different from the previous two because there were strong laser reflections off of the optical window on the wind tunnel, so the camera had to be moved to avoid permanent damage to the camera sensor from being exposed to high-intensity laser light.

The lifetime method was able to capture the same complex shock structure as the real-time method using the high-speed camera, while maintaining 1600x1200-pixel resolution. The disadvantage with this method is that the maximum camera frame rate in double-exposure mode (6 Hz) is significantly slower than the flowfield's 400 Hz natural frequency, making it very difficult to correlate each image with a specific instance in the flow to form useful videos for visualizing the flow field.

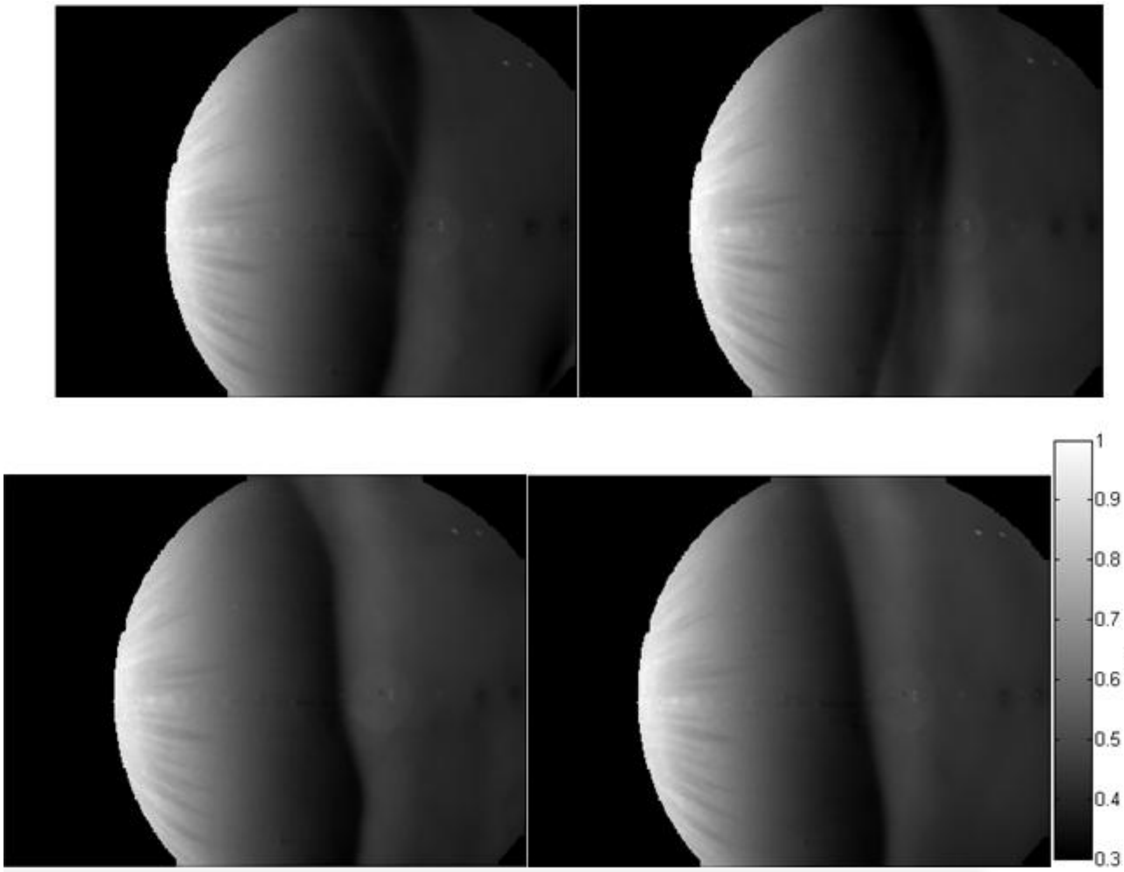

Figure 5.13 Unsteady Lifetime PSP data at Mach 0.6 (P_{ref}=71.84 kPa)

A comparison between the PSP data and the actual pressure values at corresponding azimuthal locations for the first image in Figure 5.13, obtained by the pressure taps mounted along the center of the model for the lifetime method, is shown in Figure 5.14. Like the previous test methods, the PSP data correlates very well with the pressure tap data at the front and mid-sections of the model, but deviates near the aft section due to the PSP's response to the temperature gradient. The x-axis of this plot is slightly different from the Figure 5.7 and Figure 5.12 since the viewing angle is slightly different for this test method.

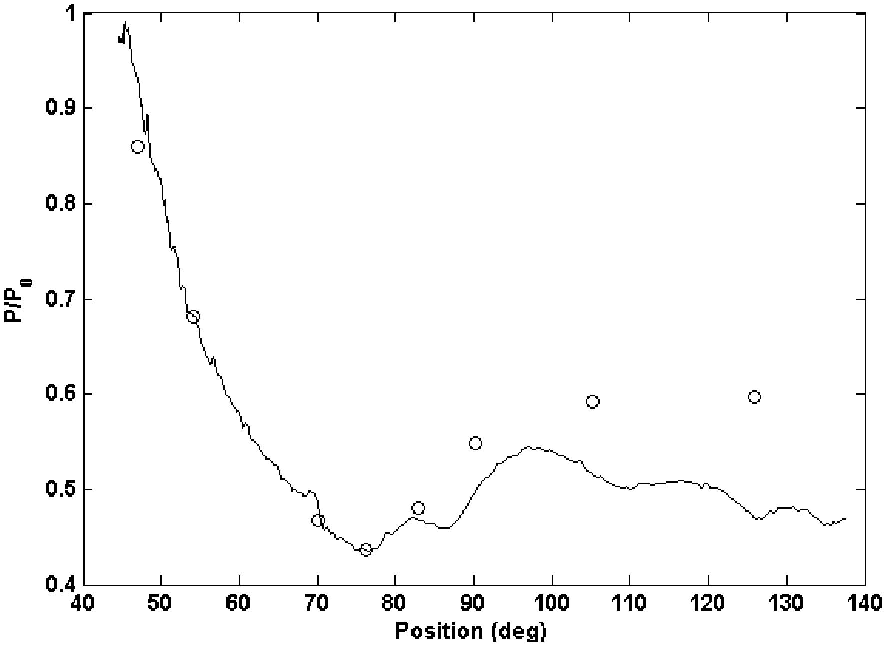

Figure 5.14 Comparison of PSP and Pressure Tap Data for Lifetime Method

Chapter 6 : Discussion

6.1 Uncertainty

Comparing the PSP results obtained using the phase-averaging technique in Figure 5.2, the real-time technique in Figure 5.11, and the lifetime method in Figure 5.13, differences in data quality can be readily seen simply from the differences in the noise level of the data sets. The uncertainty in PSP measurements depends on the accuracy of the measured changes in light intensity, which is limited by the measurement noise.[2] The noise in the measurement is mainly attributed to the photodetector and the illumination source. The major sources for camera noise include photon shot noise, dark-charge noise, and read noise. Ideally, the illumination source is required to produce spatially-uniform light over the model to avoid intensity changes due to model deformation or movement between the wind-on and wind-off images. The overall intensity of the illumination must be repeatable between images.

For this work, the photon shot noise and read noise is unavoidable since they are inherent to the photodetector itself, but can be lowered by using a scientific-grade CCD camera with high quantum efficiency. The main disadvantage of these cameras is the high cost. The dark-charge noise can be reduced to very low levels by capturing a series of dark images and subtracting them from the data, thus retaining only the luminescence signal. Other random noise sources characteristic of the imager can be reduced by image averaging and spatial averaging.

Calculation of the signal-to-noise ratio (SNR) in this work required the measurement of the signal and noise components over a region of interest in multiple identical images.

A 10-pixel by 10-pixel area at the front of the model where minimal pressure gradients were present was chosen to calculate the variation of each pixel between 20 images. The mean value of the pixel intensities was taken as the signal component, while the standard deviation was taken as the noise. Applying this method, the SNR for the phase-averaged, real-time, and lifetime techniques were determined to be 47.8, 6.02, and 24.6, respectively. The SNR results obtained by averaging four images, in the phase-averaging technique, almost doubled those obtained using the lifetime technique, where no averaging was applied. The source of noise varies for each different experimental method, and will be discussed next. Fortunately, there are solutions available to reduce or eliminate these errors. Many of these corrections have been applied and will also be discussed.

One of the most important causes of error for any pressure-sensitive paint system is the paint application. Ideally, the paint layer should be applied very uniform over the model, while strong enough to withstand aerodynamic loading. To ensure the best possible paint application for these tests, an airbrush was used to evenly spray several thin coats of paint over the model surface. The same paint application was used for all data presented herein. Thus, any error due to paint would be present for all methods.

Sources of Errors for Phase-averaging Technique

For the phase-averaging technique, one error source often encountered is due to false pressure data resulting from model movement between wind-on and wind-off images. Typically, image registration techniques are used during the data reduction process to ensure proper alignment of the two images. For this experiment, much of the image alignment errors were corrected by mounting the cameras on the wind tunnel, so that the camera could move with the wind tunnel. In the results presented in Figure 5.2, Figure 5.11, and Figure 5.13, no image registration problems are observed.

Due to the unsteady fluctuations in the shedding frequency and amplitude, the total amount of light during each camera exposure will vary because of frequency jitter. To minimize the error caused by the illumination source, two LED arrays were used to provide uniform lighting over the entire model. Also, a digital pulse counter was used to count the number of light pulses illuminating the model at each phase delay. This pulse count was applied to each image to correct the overall intensity to a baseline value. Using this method, the total amount of light pulses for each captured image at each delay was not allowed to vary by more than 5% of the total number of pulses received by the first image.

A third cause for error is caused by calibration errors due to the detection angle. Bencic had reported that at viewing angles beyond 70°, the variations in the calibration coefficients reached 3% and continues to increase with the viewing angle.[55] A pixel-by-pixel calibration was performed on the luminescence intensity images to counteract these errors.

Finally, photodegradation is another source for potential errors. To minimize these effects, the excitation sources were gated by the camera shutter, such that the lights only turned on when the camera shutter was open. Since the exposure time for each image was merely 250 ms, there was very little photodegradation in the results.

Sources of Errors for Real-time Technique

Because of the extremely short amount of time for the high-speed camera to obtain data (less than 2 seconds), errors related to photodegradation are nearly nonexistent. Also due to the fast shutter speed, the excitation light source provided continuous illumination, such that there were no light variations from image to image. Therefore, the major source of noise for this technique was caused by the shot noise of the high-speed camera, where a high shutter speed resulted in very low light levels, introducing high noise levels for each image. Since there are no averaging techniques applied to the images, neither onboard the camera nor during the data reduction process, the noise level is much higher than the data obtained by the phase-averaging technique.

Sources of Errors for Lifetime Technique

Many sources of error associated with model deformation and non-uniform illumination for intensity-based phase-averaging PSP measurements do not exist in lifetime-based PSP methods. Since all the required intensity information is acquired from one single pulse of laser light, any errors caused by non-uniformities of the illumination and paint application can theoretically be eliminated. However, wind-off images are still required to counteract calibration errors discussed earlier. Although a wind-off image is needed for this method, by mounting the camera on the wind tunnel image registration errors are minimized. The major uncertainty in the lifetime-based method in this experiment is photon-shot-noise of the camera sensor. The photon-shot-noise is limited by the pressure uncertainty, which is given by Liu and Sullivan[5]:

$$\frac{(\Delta P)}{(P)} = \frac{1}{\sqrt{n_{pe\max}}} \frac{1}{K_{sv} P} \frac{1-\exp\left[-(1+K_{sv}P)\left(t_g/\tau\right)\right]}{\left(t_g/\tau\right)\exp\left[-0.5(1+K_{sv}P)\left(t_g/\tau\right)\right]} \tag{6.1}$$

Where $K_{sv} = B/(AP_{ref})$, A, and B are Stern-Volmer coefficients. t_g is the exposure time for Gate 1. n_{pemax} is the number of photoelectrons collected in one gate interval. The above equation shows that the pressure uncertainty is a function of the Stern-Volmer coefficients, the exposure time of Gate 1, and the pressure.

Another potential error source for measurements involving laser systems is laser-speckle, which is a pattern of random light intensity variations. This issue is eliminated by taking a ratio of the ratios, because two sets of images are acquired from the same laser pulse using the same optical elements and the same camera. So each image contains the same speckle pattern, which can be removed by taking a ratio of these images.

6.2 Comparison of Methods

Each of the data acquisition techniques has its own advantages and disadvantages. The phase-averaging method is the most conventional method, since it has been used extensively in past experiments. It has the ability to provide the experimenter with high spatial resolution data that captures the events within one period of the flow oscillation. However, the captured data may lose certain details in the flow due to the averaging. The phase-averaging technique also introduced errors caused by light intensity variations from image to image due to the triggering instrumentation, but can be corrected to some extentduring post-processing. The real-time technique using a high-speed camera is the simplest method to set up, and the quickest in obtaining data. It has the ability to capture every event in the flow field without any type of averaging, and can capture hundreds of oscillation periods within a couple of seconds. Although this technique can present the experimenter with very useful data in the flow field, there is a significant increase in shot noise and a decrease in image resolution compared to the phase-averaging technique. Finally, the single-shot lifetime method has the ability to capture the same flow field as the high-speed camera, without the use of Kulite pressure transducers for phase locking, while maintaining the higher image resolution. This is extremely useful in cases where the location of the pressure gradient is unknown or the pressure change is very small. However, the data are captured at random times with respect to the flow period, making it difficult for the experimenter to study the development of the flow over time.

6.3 Flow Phenomena

All three different methods revealed a shock structure close to the apex of the hemisphere. Upon close inspection of Figure 5.7, Figure 5.12, and Figure 5.14, the flow separation occurs just behind that region, at about 95° relative to the base of the model. Similar findings were reported by Vukasinovic et al., who observed separation at around 100° over a hemispherical turret model placed in M = 0.64 flow using Malley probe measurements and hot-wire anemometry.[52] In that experiment, they found that at M = 0.64, the flow on top of the hemispherical dome becomes supersonic and creates an unsteady straight shock located at the top of the hemisphere. This shock causes the boundary layer to separate prematurely over the hemisphere, creating the strong separation at the back of the model.[52] This separation could be clearly observed in the temperature gradient in Figure 5.3. This temperature gradient was also sensed by the PSP, producing errors in the final pressure data.

Both the real-time and lifetime methods were able to capture features in the flow field that were not visible in the phase-averaging technique, such as the asymmetrical oscillation of pressure gradients shown in Figure 5.11 and Figure 5.13. The combinations of the symmetric and asymmetric pressure gradients are governed by large-scale vortices shed from the top and the sides of the model and have been the subject of many studies. In one of the earliest studies on the wake structure behind a sphere, Taneda proposed that the vortex shed from a sphere begins to rotate asymmetrically about the streamwise axis from $Re=5\times10^5$.[45] Using Large Eddy Simulation (LES) to study the vortex shedding from a hemisphere at Re = 150,000, Manhart stated that the vortex shedding from the top surface is due to roll up of the shear layer bounding the separation region behind the hemisphere, and the antisymmetric shedding from the side faces results from an interaction of the shear layers bounding the separation region in the lateral direction.[58] In a later study, Yun, Kim, and Choi used large eddy simulations and found large-scale waviness of vertical structures in the wake of a hemispherical dome at Reynolds numbers greater than 10^4.[59] They concluded that these oscillations were likely to be caused by the tilting of the vortices generated by the shear-layer instabilities due to the varying convection velocities along the azimuthal direction.

Although most results reported on the flow phenomena around hemispherical domes were done at lower Reynolds numbers than the flow conditions in this study, the scientists all observed different degrees of asymmetrical pressure characteristics in the wake of the model. At the moment, it is difficult to conclude what are the causes for the asymmetrical oscillations observed over the surface of the model without more knowledge of what is happening behind and around the wake of the hemispherical dome at similar test conditions.

Chapter 7 : Conclusion

In this work, the porous pressure-sensitive paint technique was successfully applied in an unsteady test on a model placed in an industrial wind tunnel. The global, unsteady surface pressure distribution on a hemispherical dome in Mach 0.6 flow and $P_0 = 71.8$ kPa was successfully resolved using three different PSP measurement techniques: phase-averaging, real-time, and lifetime single-shot methods. The techniques revealed a shock wave structure near the apex of the model, oscillating at 400 Hz, proving the polymer/ceramic PSP with PtTFPP luminophore to be an effective tool for studying the unsteady surface pressure in such a flow. An assessment of the data quality of each data-acquisition technique was discussed, including the calculation of the SNR, the sources for the errors, and the flow phenomenon captured by each method. Future work will focus on correcting temperature effects in the PSP data by using a model made from a homogeneous material with high thermal conductivity, so that the influence of nonuniform heat flux and the resulting temperature gradients will be reduced. Since the lifetime method has the highest spatial resolution of the three techniques, further improvements will be made to resolve the images with respect to their time of acquisition. For future work, several techniques could be implemented to minimize some of the errors discussed in this paper. First, certain temperature effects in the PSP data can be corrected to some extent by using a model made from a homogenous material with high thermal conductivity, so that the surface temperature of the model can remain constant throughout. Secondly, to minimize temperature effects over the model caused by flow separation, PSP can be used in combination with TSP. Since PSP is sensitive to both pressure and temperature, while TSP is pressure insensitive, the temperature gradient obtained using the TSP can be used to correct for temperature errors in the PSP. Out of three data acquisition techniques, the lifetime-based single-shot method provided the experimenter with the highest spatial resolution; further improvements can be made to resolve the images with respect to their time of acquisition. Finally, to understand the causes for the asymmetric flow structures around the shock and separation locations over the dome, methods such as PIV could be used to study the flow beyond the model surface.

References

1. Morris, M.J., Donovan, J.F., Kegelman, J.T., Schwab, S.D., Levy, R.L., and Cites, R.C., "Aerodynamic Applications of Pressure Sensitive Paint," *AIAA Journal,* No. 31, 1993.

2. Bell, J.H., Schairer, E.T., Hand, L.A., and Mehta, R.D., "Surface Pressure Measurements Using Luminescent Coatings," *Annu. Rev. Fluid Mech.,* Vol. 33, 2001, pp. 155-206.

3. Gregory, J.W., Asai, K., Kameda, M., Liu, T., and Sullivan, J.P., "A Review of Pressure-Sensitive Paint for High-Speed and Unsteady Aerodynamics," *Proceedings of the Institution of Mechanical Engineers, Part G: Journal of Aerospace Engineering,* Vol. 222, No. 2, 2008, pp. 249-290.

4. Liu, T., Campbell, B.T., Burns, S.P., and Sullivan, J.P., "Temperature- and Pressure-Sensitive Luminescent Paints in Aerodynamics," *Applied Mechanics Reviews,* Vol. 50, No. 4, 1997.

5. Liu, T., and Sullivan, J.P., "Pressure and Temperature Sensitive Paints," Springer, New York, 2005.

6. Puklin, E., Carlson, B., Gouin, S., Costin, C., Green, E., Ponomarev, S., Tanji, H., and Gouterman, M., "Ideality of Pressure-Sensitive Paint. 1. Platinum Tetra (Pentaflourophenyl) Porphine in Flouracrylic Polymer," *Journal of Applied Polymer Science,* Vol. 70, 1999.

7. Goss, L., Jones, G., Crafton, J., and Fonov, S., "Temperature Compensation for Temporal (Lifetime) Pressure Sensitive Paint Measurements," *43rd Aerospace Sciences Meeting and Exhibit,* AIAA-2005-1027, American Institute of Aeronautics and Astronautics, Reno, NV, 2005.

8. Engler, R.H., Klein, C., and Trinks, O., "Pressure Sensitive Paint Systems for Pressure Distribution Measurements in Wind Tunnels and Turbomachines," *Measurement Science and Technology,* No. 11, 2000.

9. Bell, J.H., and McLachlan, B.G., "Image Registration for Pressure-Sensitive Paint Applications," *Experiments in Fluids,* Vol. 22, No. 1, 1996.

10. Yamashita, T.N., Asai, K., Singh, M., and Naughton, N.M., "Pressure-Sensitive Paint Measurement of Unsteady Pressure Field behind an Oscillating Fence Actuator," *Proceedings of the 13th International Symposium on Flow Visualization,* ISFV13 (130), 2008.

11. Goss, L., Trump, D., Sarka, B., Lydick, L., and Baker, W., "Multi-Dimensional Time-Resolved Pressure-Sensitive Paint Techniques: A Numerical and Experimental Comparison," *37th Aerospace Sciences Meeting and Exhibit,* AIAA-2000-0832, American Institute of Aeronautics and Astronautics, Reno, NV, 1999.

12. Gregory, J.W., Sakaue, H., and Sullivan, J.P., "Fluidic Oscillator as a Dynamic Calibration Tool," *22nd Aerodynamic Measurement Technology and Ground Testing Conference,* AIAA 2002-2701, 2002.

13. Gregory, J.W., "Porous Pressure-Sensitive Paint for Measurement of Unsteady Pressures in Turbomachinery," *42nd AIAA Aerospace Sciences Meeting and Exhibit,* AIAA 2004-0294, American Institute of Aeronautics and Astronautics, Reno, NV, 2004.

14. Nakakita, K., "Unsteady Pressure Distribution Measurement Around 2D-Cylinders Using Pressure-Sensitive Paint," *25th AIAA Applied Aerodynamics Conference,* AIAA 2007-3819, American Institute of Aeronautics and Astronautics, Miami, FL, 2007.

15. Sakamura, Y., Matsumoto, M., and Suzuki, T., "High Frame-rate Imaging of Surface Pressure Distribution Using a Porous Pressure-sensitive Paint," *Measurement Science & Technology,* Vol. 16, No. 3, 2005.

16. Kameda, M., Tabei, T., Nakakita, K., Sakaue, H., and Asai, K., "Image Measurements of Unsteady Pressure Fluctuation By a Pressure-sensitive Coating on Porous Anodized Aluminum," *Measurement Science & Technology,* Vol. 16, No. 12, 2005.

17. Wong, O.D., Watkins, A.N., and Ingram, J.L., "Pressure-Sensitive Paint Measurements on 15% Scale Rotor Blades in Hover," *35th AIAA Fluid Dynamics Conference and Exhibit,* AIAA 2005-5008, 2005.

18. Wong, O.D., Noonan, K.W., Watkins, A.N., Jenkins, L.N., and Yao, C., "Non-Intrusive Measurements of a Four-Bladed Rotor in Hover - A First Look," *AHS Specialists' Conference on Aeromechanics,* 2010.

19. Gregory, J.W., Kumar, P., Peng, D., Fonov, S., Crafton, J., and Liu, T., "Integrated Optical Measurement Techniques for Investigations of Fluid-Structure Interactions," *39th AIAA Fluid Dynamics Conference,* AIAA 2009-4044, American Institute of Aeronautics and Astronautics, San Antonio, TX, 2009.

20. Kumar, P., "Development of a Single-Shot Lifetime PSP Measurement Technique for Rotating Surfaces," *M.S. Thesis,* The Ohio State University, Columbus, OH, 2010.

21. Gregory, J.W., and Sullivan, J.P., "Effect of Quenching Kinetics on Unsteady Response of Pressure-Sensitive Paint," *AIAA Journal,* Vol. 44, No. 3, 2006, pp. 634-645.

22. Winslow, N.A., Carroll, B.F., and Kurdila, A.J., "Model Development and Analysis of the Dynamics of Pressure-Sensitive Paints," *AIAA Journal,* Vol. 39, No. 4, 2001.

23. Kameda, M., and Asai, K., "PSP/TSP," *Noninvasive and Visualizing Techniques,* (in Japanese) (Eds S. Ogawa and T. Ueno), 2007 (NTS, Tokyo).

24. Gouin, S., and Gouterman, M., "Ideality of Pressure-Sensitive Paint II. Effect of Annealing on the Temperature Dependence of the Luminescence," *Journal of Applied Polymer Science,* Vol. 7, No. 13, 2000.

25. Schanze, K.S., Carroll, B.F., Korotkevitch, S., and Morris, M.J., "Temperature Dependence of Pressure Sensitive Paints," *AIAA Journal,* Vol. 35, No. 2, 1997.

26. Mebarki, Y., Cooper, K.R., and Reichert, T.M., "Automotive Testing Using Pressure-Sensitive Paint," *Journal of Visualization,* Vol. 6, No. 4, 2003.

27. Basu, B.J., Anandan, C., and Rajam, K.S., "Study of the Mechanism of Degradation of Pyrene-Based Pressure Sensitive Paints," *Sensors and Actuators B: Chemical,* Vol. 94, No. 3, 2003.

28. Schairer, E.T., "Optimum Thickness of Pressure-Sensitive Paint For Unsteady Measurements," *AIAA Journal,* Vol. 40, No. 11, 2002.

29. Asai, K., Kanda, H., Cunningham, C.T., Erausquin, R., and Sullivan, J.P., "Surface Pressure Measurements In a Cryogenic Wind tunnel By Using Luminescent Coatings," *17th International Congress on Instrumentation in Aerospace Simulation Facilities,* Institute of Electrical and Electronics Engineers Inc., Piscataway, NJ, 1997., pp. 105-114.

30. Asai, K., Amao, Y., Iijima, Y., Okura, I., and Nishide, H., "Novel Pressure-sensitive Paint for Cryogenic and Unsteady Wind Tunnel Testing," *21st AIAA Aerodynamic Measurement Technology and Ground Testing Conference,* AIAA 2000-2527, American Institute of Aeronautics and Astronautics, Denver, CO, 2000.

31. Erausquin, R., Cunningham, C.T., Sullivan, J.P., Asai, K., Kanda, H., Kunimasu, T., and Iijima, Y., "Cryogenic Pressure Sensitive Fluorescent Paint Systems," *36th AIAA Aerospace Sciences meeting and Exhibit,* AIAA 98-0588, 1998.

32. Fang, S., Long, S.R., Disotell, K.J., Gregory, J.W., Semmelmayer, F.C., and Guyton, R.W., "Comparison of Unsteady Pressure-Sensitive Paint Measurement Techniques,"

27th AIAA Aerodynamic Measurement Technology and Ground Testing Conference, AIAA 2010-4919, American Institute of Aeronautics and Astronautics, Chicago, IL, 2010.

33. Baron, A.E., Danielson, J.D.S., Gouterman, M., Wan, J.R., Callis, J.B., and McLachlan, B., "Submillisecond Response Times of Oxygen-Quenched Luminescent Coatings," *Review of Scientific Instruments,* Vol. 64, No. 12, 1993.

34. Sakaue, H., Sullivan, J.P., Asai, K., Iijima, Y., and Kunimasu, T., "Anodized Aluminum Pressure Sensitive Paint in a Cryogenic Wind Tunnel," *Proceedings of the 45th International Instrumentation Symposium,* 1999.

35. Scroggin, A.M., Slamovich, E.B., Crafton, J.W., Lachendo, N., and Sullivan, J.P., "Porous Polymer/Ceramic Composites for Luminescent-Based Temperature and Pressure Measurement," *Material Research Society Proceedings,* Vol. 560, 1999, pp. 347-352.

36. Gregory, J.W., Sakaue, H., and Sullivan, J.P., "Unsteady Pressure Measurements in a Turbocharger Compressor Using Porous Pressure-sensitive Paint," *Proceedings of the 40th AIAA Aerospace Sciences Meeting and Exhibit,* AIAA 2002-0084, American Institute of Aeronautics and Astronautics, Reston, VA, 2002.

37. Sakaue, H., and Sullivan, J.P., "Time Response of Anodized Aluminum Pressure-Sensitive Paint," *AIAA Journal,* Vol. 39, No. 10, 2001.

38. Carroll, B.F., Abbitt, J.D., Lukas, E.W., and Morris, M.J., "Step Response of Pressure-Sensitive Paints," *AIAA Journal,* Vol. 34, No. 3, 1996.

39. Bencic, T., "Dynamic Calibration Rig for Pressure-Sensitive Paints at NASA Glenn Research Center," *8th Annual Pressure-Sensitive Paint Workshop,* 2000.

40. Davis, P.A., and Zasimowich, R.F., "High Frequency Dynamic Pressure Calibration Technique," *Proceedings of the 31st International Instrumentation Symposium,* 85-0109, Vol. 31, 1985.

41. McGraw, C.M., Shroff, H., Khalil, G., and Callis, J.B., "The Phosphorescence Microphone: A Device for Testing Oxygen Sensors and Films," *Review of Scientific Instruments,* doi: 10.1063/1.1626009, Vol. 74, 2003.

42. Winslow, N.A., Carroll, B.F., and Setzer, F.M., "Frequency Response of Pressure Sensitive Paints," *27th AIAA Fluid Dynamics Conference,* AIAA 96-1967, 1996.

43. McGraw, C.M., Bell, J.H., Khalil, G., and Callis, J.B., "Dynamic surface pressure measurements on a square cylinder with pressure sensitive paint," *Experiments in Fluids,* Vol. 40, No. 2, 2006.

44. Vukasinovic, B., Brzozowski, D., Glezer, A., Bower, W.W., and and Kibens, V., "Separation Control over a Surface-Mounted Hemispherical Shell," *35th AIAA Fluid Dynamics Conference and Exhibit,* AIAA 2005-4878, 2005.

45. Taneda, S., "Visual Observations of the Flow Past a Sphere at Reynolds Numbers Between 10^4 and 10^6," *Journal of Fluid Mechanics,* Vol. 85, No. 1, 1978.

46. Sakamoto, H., and and Haniu, H., "A Study on Vortex Shedding From Spheres in a Uniform Flow," *Journal of Fluids Engineering,* Vol. 112, 1990.

47. Gordeyev, S., and Jumper, E.J., "Fluid Dynamics and Aero-Optics of Turrets," *Progress in Aerospace Sciences,* Vol. 46, No. 8, 2010, pp. 388-400.

48. Fitzgerald, E.J., and Jumper, E.J., "The Optical Distortion Mechanism in a Nearly Incompressible Free Shear Layer," *Journal of Fluid Mechanics,* Vol. 512, 2004.

49. Purhoit, S.C., Shang, J.S., and Hankey, W.L., "Effect of Suction on the Wake Structure of a Three-Dimensional Turret," *AIAA Paper,* AIAA 83-1738, 1983.

50. Snyder, C.H., Franke, M.E., and Masquelier, M.L., "Wind-tunnel Tests of an Aircraft Turret Model," *Journal of Aircraft,* Vol. 37, 2000.

51. Gordeyev, S., Post, M.L., McLaughlin, T., Ceniceros, J., and Jumper, E.J., "Aero-optical Environment Around a Conformal Window Turret," *AIAA Journal,* Vol. 45, 2007.

52. Vukasinovic, B., Glezer, A., Gordeyev, S., Jumper, E., and and Kibens, V., "Active Control and Optical Diagnostics of the Flow Over a Hemispherical Turret," *46th Aerospace Science Meeting and Exhibit,* AIAA 2008-0598, 2008.

53. Fang, S., Disotell, K.J., Gregory, J.W., Semmelmayer, F.C., and Guyton, R.W., "Unsteady Surface Pressure Measurements on a Hemispherical Dome with Pressure-Sensitive Paint," *10th International Conference on Fluid Control, Measurements, and Visualization,* 2009.

54. The Cooke Corporation, "PCO Camera Timing Issues," 2005.

55. Bencic, T.J., "Calibration of Detection Angle for Full Field Pressure-Sensitive Paint Measurements," *39th AIAA Aerospace Sciences Meeting & Exhibit,* AIAA 2001-0307, 2001.

56. Gregory, J.W., Sullivan, J.P., Wanis, S., and Komerath, N.M., "Pressure-Sensitive Paint as a Distributed Optical Microphone Array," *Journal of the Acoustical Society of America,* Vol. 119, No. 1, 2006, pp. 251-261.

57. Covington, M., *Digital SLR Astrophotography,* Cambridge University Press, New York, 2007, pp. 22-23.

58. Manhart, M., "Vortex Shedding From a Hemisphere in a Turbulent Boundary Layer," *Theoretical and Computational Fluid Dynamics,* Vol. 12, No. 1, 1998.

59. Yun, G., Kim, D., and Choi, H., "Vortical Structures Behind a Sphere at Subcritical Reynolds Numbers," *Physics of Fluids,* Vol. 18, 2006.

Appendix A: AC Response of Pressure transducer and PSP

420 Hz:

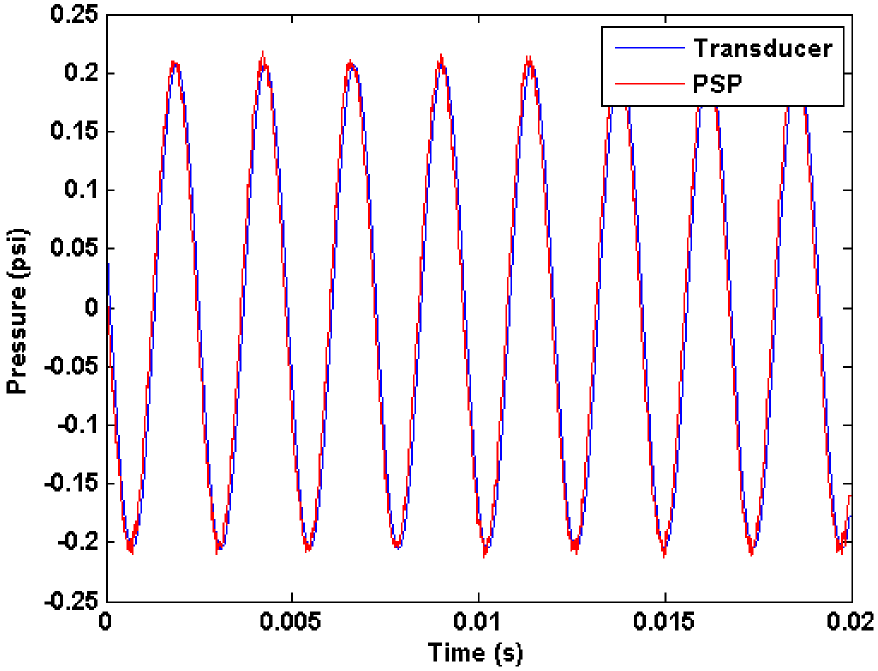

530 Hz:

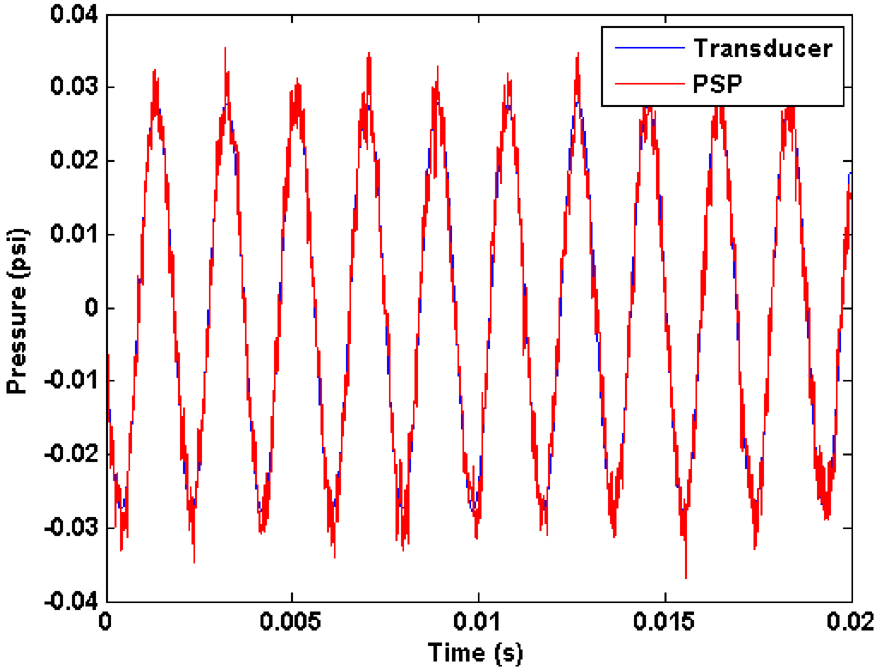

720 Hz:

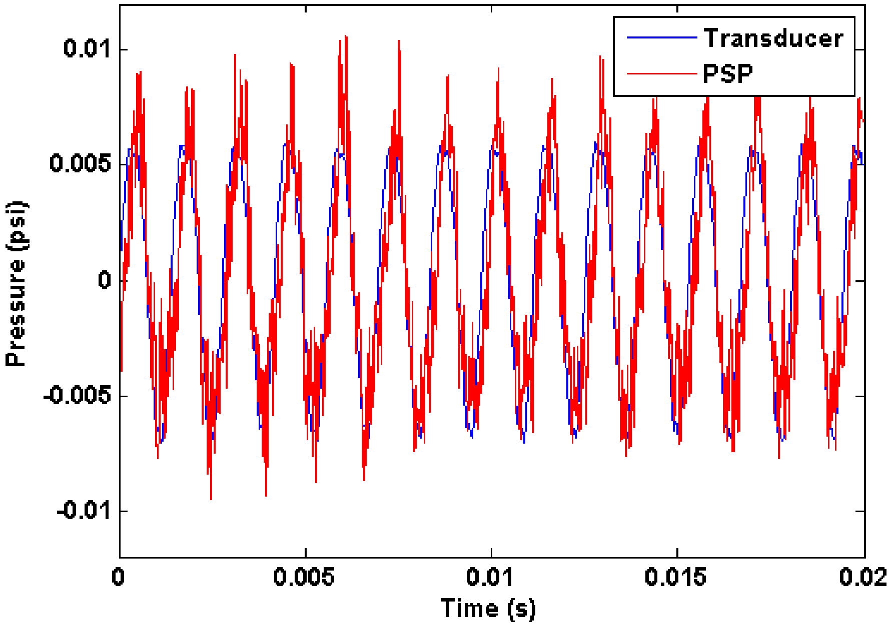

1020 Hz:

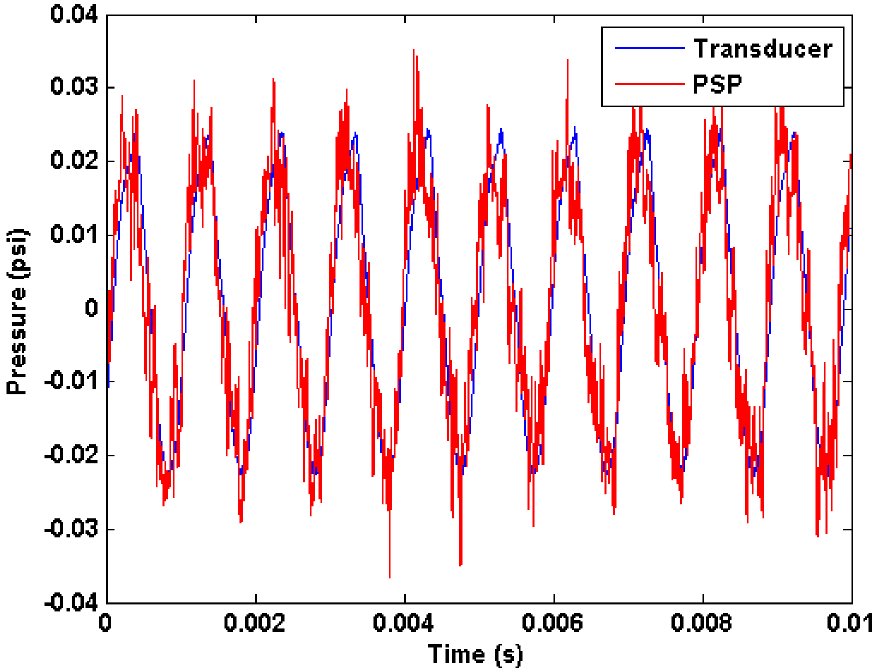

1100 Hz:

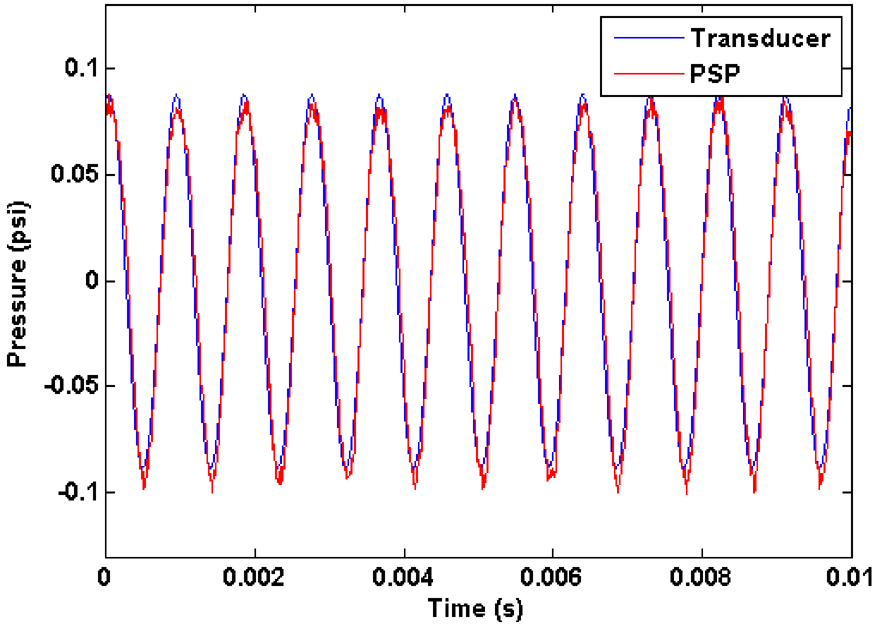

1460 Hz:

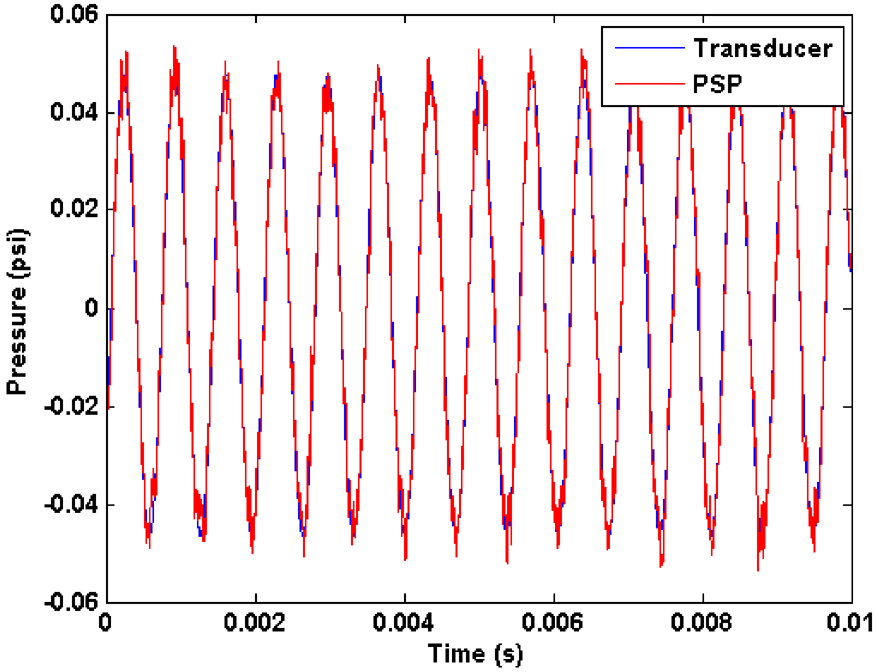

1910 Hz:

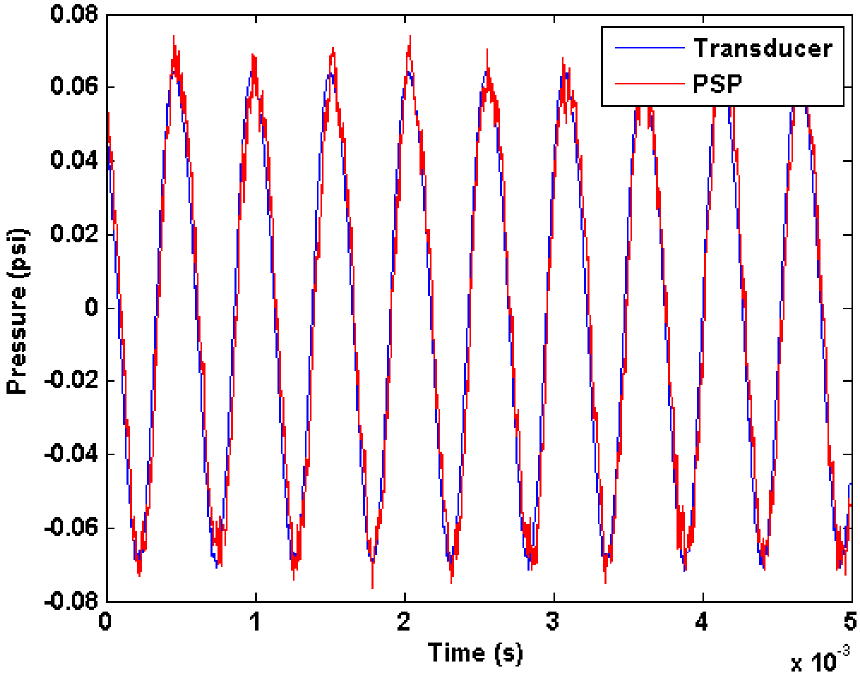

2410 Hz:

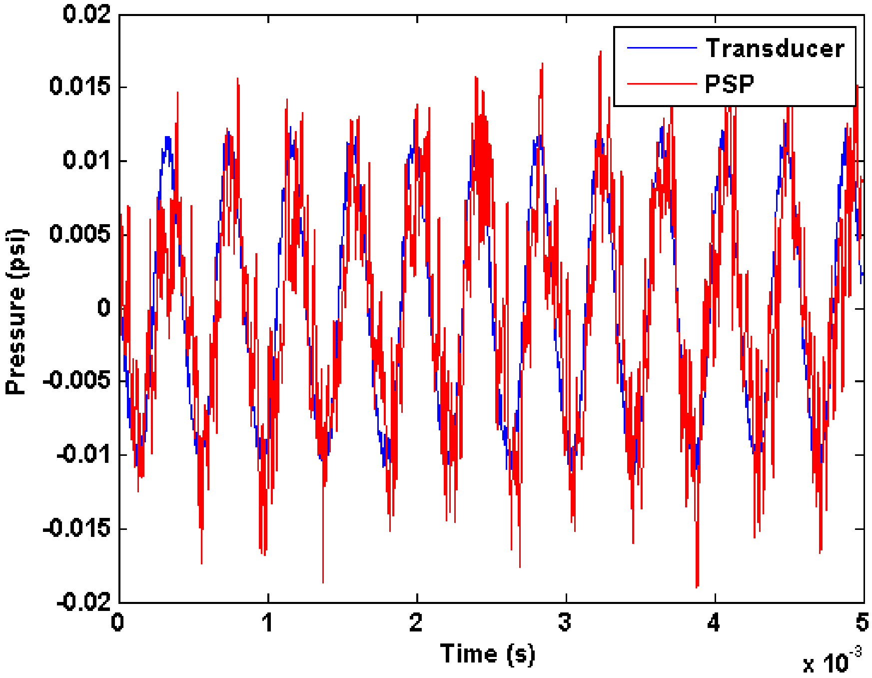

2640 Hz:

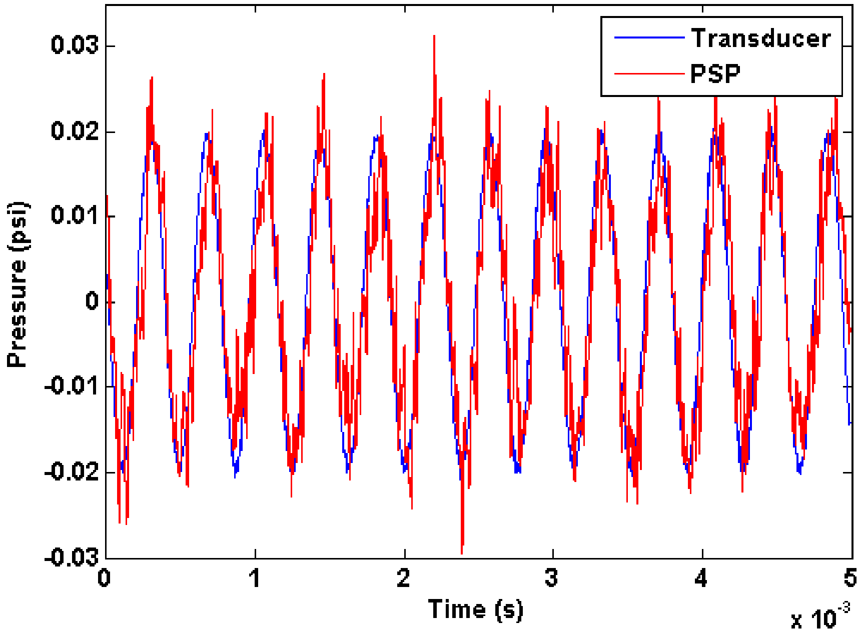

2700 Hz:

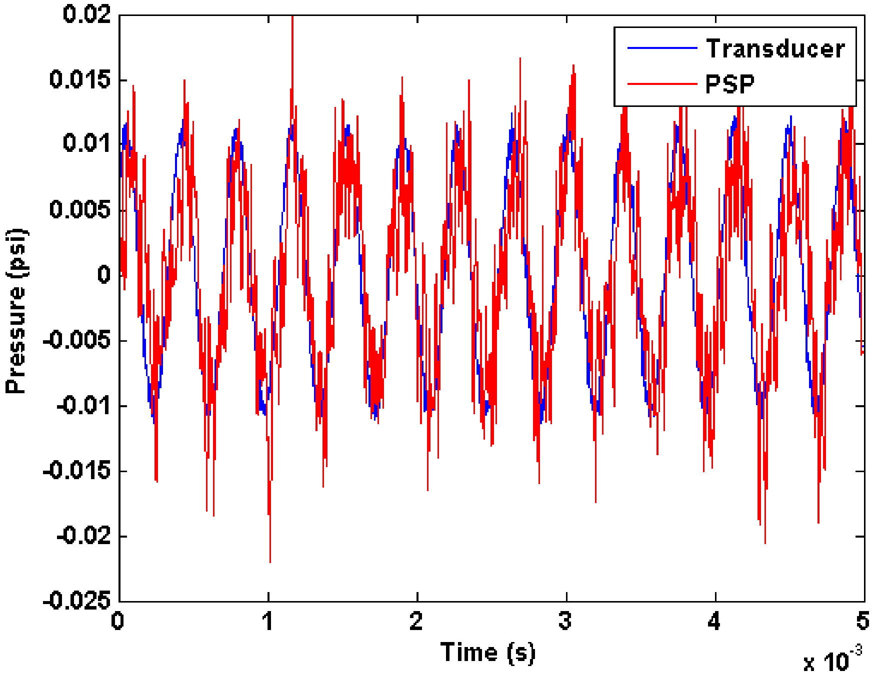

2800 Hz:

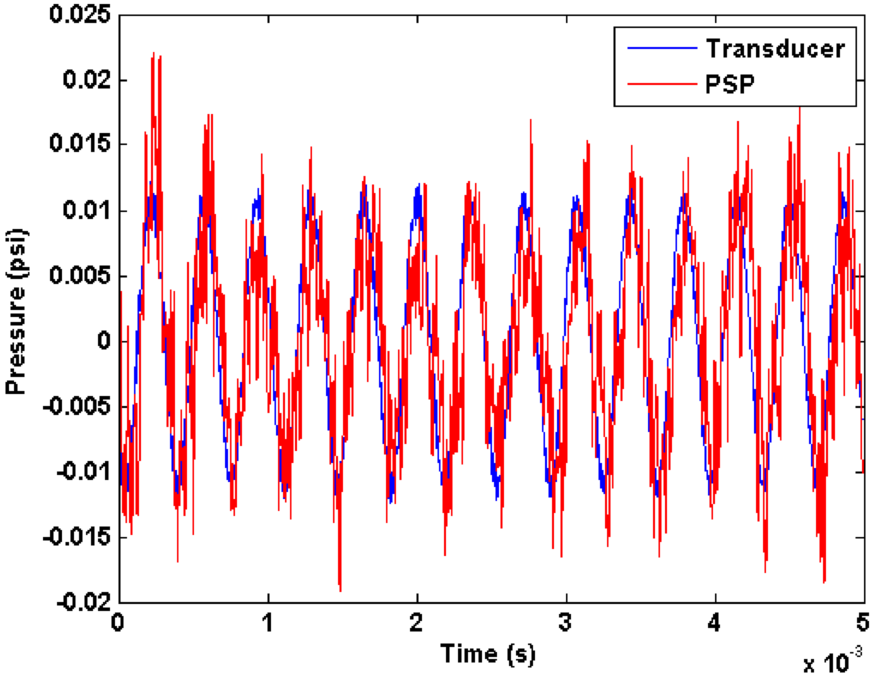

2960 Hz:

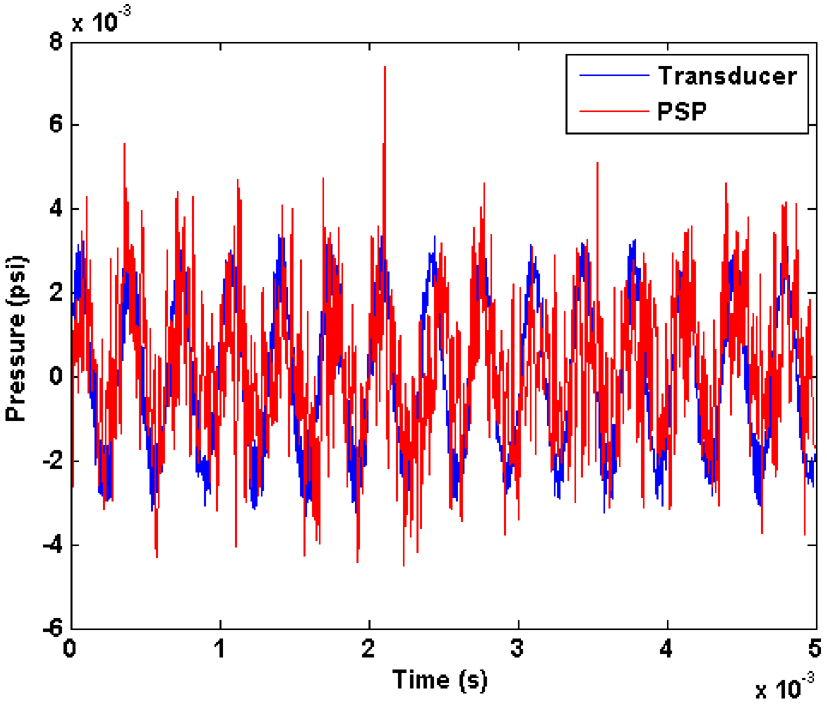

3260 Hz:

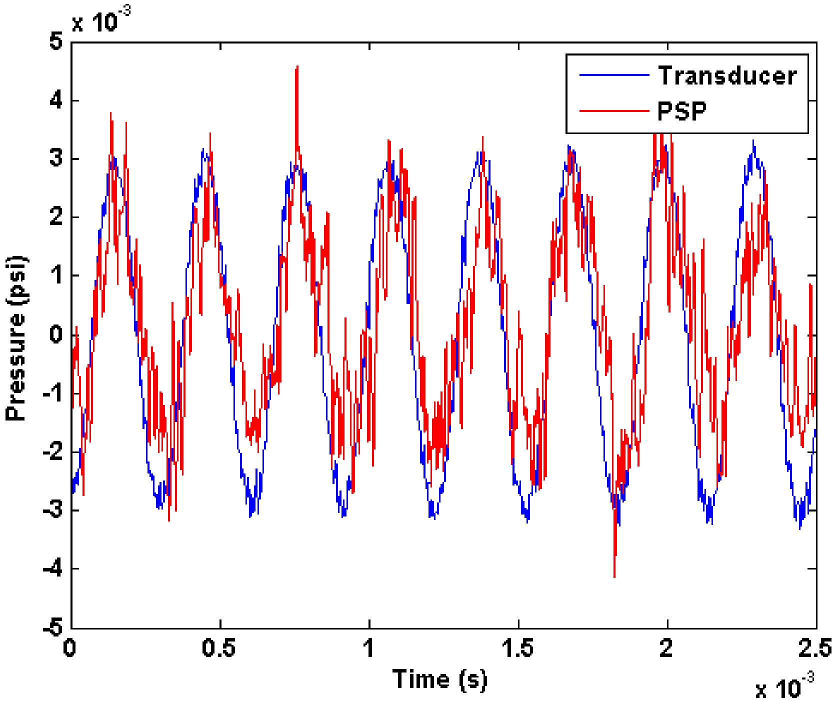

3820 Hz:

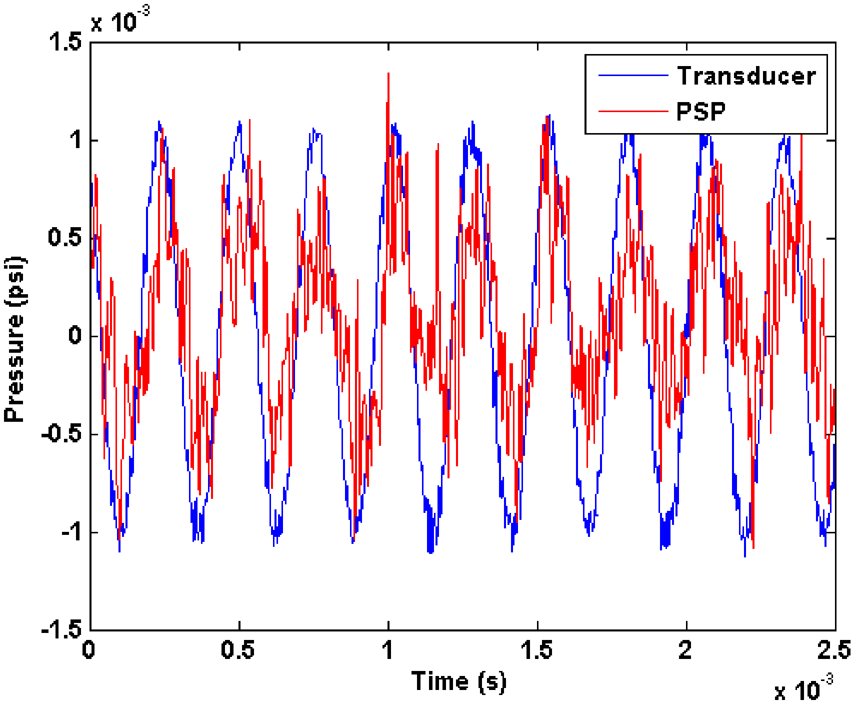

4200 Hz:

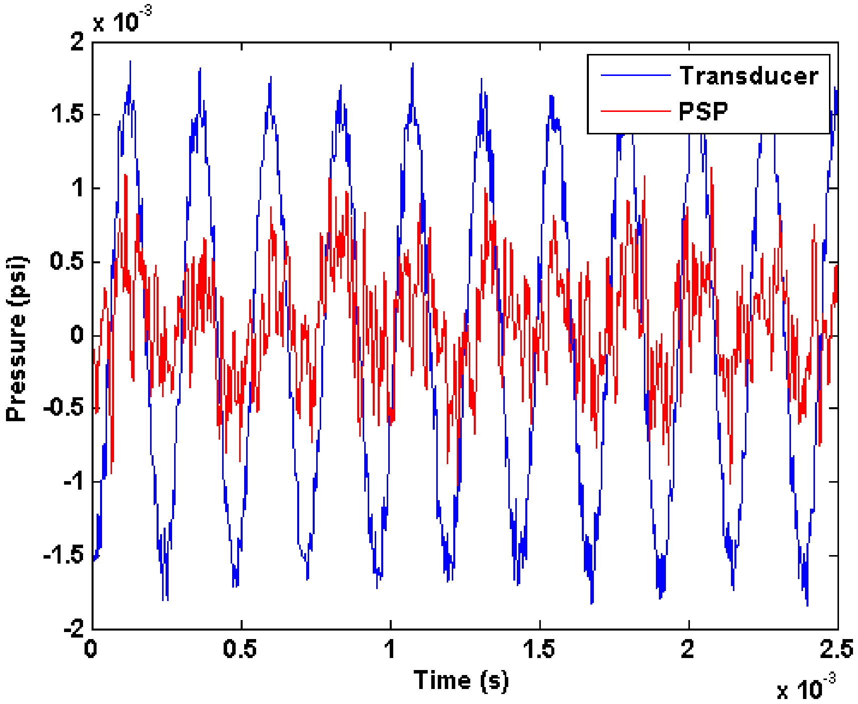

4600 Hz:

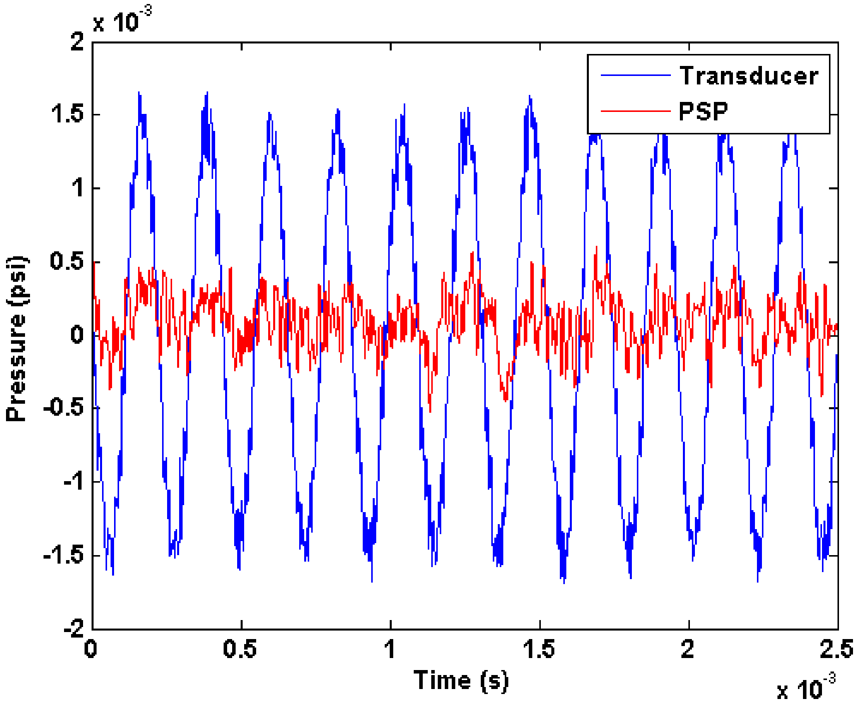

5000 Hz:

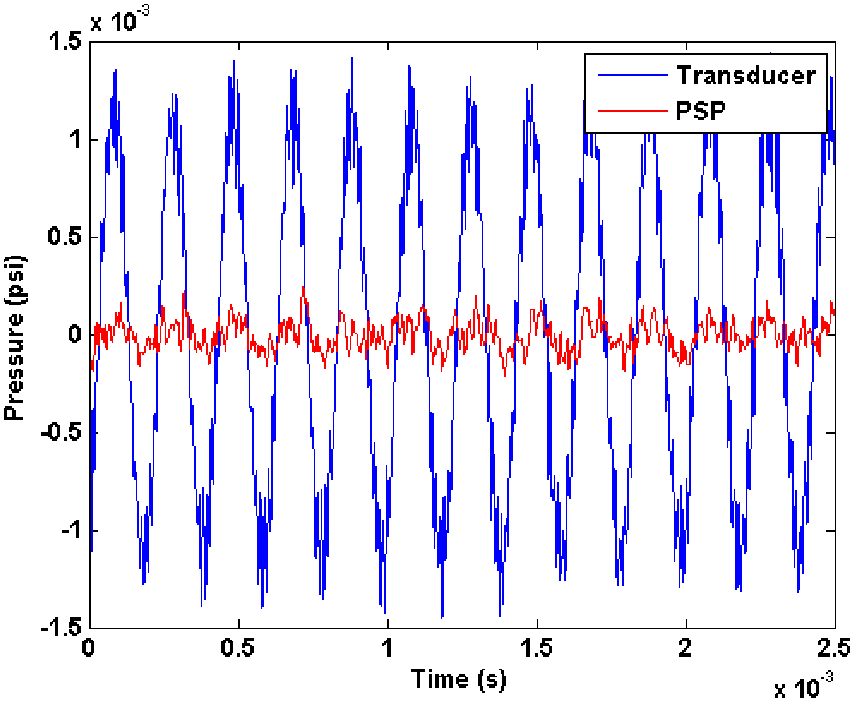
x 10^-3
1.5
1
0.5
0
-0.5
-1
-1.5
Pressure (psi)
Transducer
PSP
0
0.5
1
1.5
2
2.5
Time (s)
x 10^-3

Appendix B: Dynamic Calibration Paint Layer Thickness

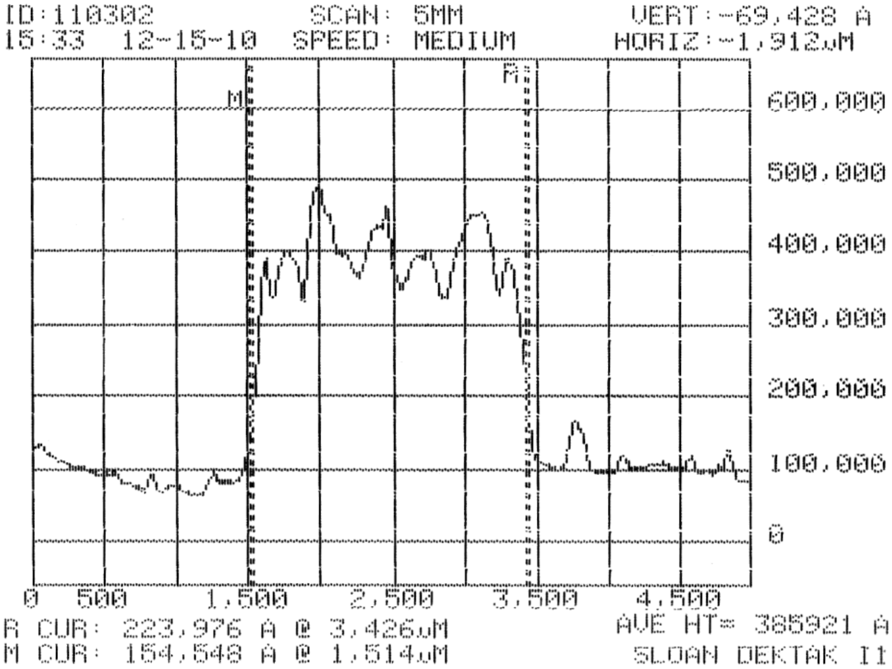

Figure B.1 Paint Layer Thickness of PSP for Dynamic Calibrations